UCLA
UCLA Previously Published Works

Title

Body Composition Metrics and Overall Survival in Head and Neck Cancer Radiotherapy

Permalink

https://escholarship.org/uc/item/0kk224n0

Journal

JAMA OTOLARYNGOLOGY-HEAD & NECK SURGERY

ISSN

2168-6181

Authors

Jank, Erika
Bang, Chulmin
Raj, Vinith B
et al.

Publication Date

2026-10-08

DOI

10.1001/jamaoto.2026.2951

Peer reviewed

eScholarship.org Powered by the California Digital Library
University of California

JAMA Otolaryngology–Head & Neck Surgery | Original Investigation

Body Composition Metrics and Overall Survival in Head and Neck Cancer Radiotherapy

Erika Jank, MS; Chulmin Bang, MD; Vinith B. Raj, MS; Jasmine Gillett, PA-C; Cesar Vincent Villafuerte III, MD; Changsuk Oh, PhD; Anthony Militchin, BA; Lydia Chau, RD; X. Sharon Qi, PhD; Robert K. Chin, MD, PhD; Kyunghyun Sung, PhD; Ricky R. Savjani, MD, PhD

IMPORTANCE Advancing the prognostication of patients with head and neck cancer who are undergoing radiotherapy may guide clinicians to better individualize support throughout oncologic treatment.

OBJECTIVE To evaluate how automated 3-dimensional soft tissue phenotyping, as extracted from routine computed tomography (CT) scans, provides deeper biological granularity into body composition and mortality risk and examine the prognostic utility of baseline body mass index.

DESIGN, SETTING, AND PARTICIPANTS This retrospective cohort study evaluated a consecutive sample of patients who were receiving conventionally fractionated definitive-intent radiotherapy for head and neck cancer between January 1, 2014, and December 31, 2024, at a single-center tertiary academic referral center. Cohort filtering was applied to exclude palliative, abbreviated, or nonstandard treatment regimens. Data were analyzed from October 2025 to May 2026.

EXPOSURES Baseline body composition metrics, including body mass index and 3-dimensional volumetric soft tissue indices, extracted automatically from pretreatment CT simulation scans using an open-source deep learning segmentation pipeline.

MAIN OUTCOMES AND MEASURES The primary outcome was overall survival. Multivariable Cox proportional hazards models were used to assess the independent prognostic associations of baseline body mass index and volumetric soft tissue indices, controlling for standard clinical confounders.

RESULTS The primary clinical cohort comprised 1187 patients (median [range] age, 64.0 [5.0-100.0] years; 323 female individuals [27.2%] and 864 male individuals [72.8%]), with an imaging subcohort of 659 patients (55.5%). While elevated body mass index categories were associated with overall survival (overweight: hazard ratio [HR], 0.70; 95% CI, 0.56-0.89; obesity: HR, 0.67; 95% CI, 0.50-0.89), a volumetric analysis revealed that this expansion was disproportionately associated with subcutaneous adiposity gain rather than muscle growth. In the imaging subcohort, elevated skeletal muscle was associated with improved overall survival (HR, 0.67; 95% CI, 0.50-0.89; $P = .001$). Conversely, elevated intermuscular adiposity was independently associated with an increased mortality risk (HR, 1.28; 95% CI, 1.03-1.58; $P = .02$).

CONCLUSIONS AND RELEVANCE The results of this cohort study suggest that higher body mass index was associated with improved overall survival. Automated volumetric CT phenotyping revealed that higher skeletal muscle and lower intermuscular adiposity were also associated with improved survival outcomes. This scalable, opportunistic framework may guide pretreatment risk stratification to identify vulnerable patients who may benefit from targeted supportive care.

JAMA Otolaryngol Head Neck Surg. doi:10.1001/jamaoto.2026.2951
Published online October 8, 2026.

Supplemental content

Author Affiliations: Department of Radiation Oncology, University of California, Los Angeles (Jank, Bang, Raj, Gillett, Villafuerte, Oh, Militchin, Chau, Qi, Chin, Savjani); University of California, Los Angeles (Oh, Sung).

Corresponding Author: Erika Jank, MS, Department of Radiation Oncology, UCLA, 200 Medical Plaza, Ste B265, Los Angeles, CA 90095 (ejank@mednet.ucla.edu).

© 2026 American Medical Association. All rights reserved, including those for text and data mining, AI training, and similar technologies.

Downloaded from jamanetwork.com by University of California - Los Angeles user on 10/08/2026

In the multidisciplinary management of head and neck cancer (HNC), preserving physiologic reserve and functional resilience throughout treatment is critical to therapeutic success.[1] Radiotherapy (RT) often exacerbates baseline vulnerabilities through toxic effects that impair oral intake, leaving patients susceptible to sarcopenia and progressive weight loss.[2-4] These physiologic changes are associated with reduced treatment tolerance and inferior overall survival (OS).[5,6] Improved methods for characterizing host vulnerability before treatment may enhance prognostication and supportive care planning in HNC.

In routine clinical practice, most centers monitor serial weight measurements throughout RT as a surrogate for treatment tolerance and nutritional decline. However, weight fluctuates substantially due to transient factors, like hydration status and treatment-related fluid shifts.[2] Body mass index (BMI; calculated as weight in kilograms divided by height in meters squared) remains a robust, widely used anthropometric measure because of its simplicity and accessibility. Although elevated BMI is associated with cardiovascular mortality and metabolic disease, several oncology studies paradoxically demonstrate improved survival among patients with higher pretreatment BMI.[7,8] However, BMI lacks the biological granularity to distinguish skeletal muscle from adipose tissue, obscuring the role of specific soft tissue compartments in treatment tolerance and survival.[9] Prior studies that evaluated BMI and nutritional status in HNC were frequently limited by relatively small cohorts, inconsistent stratification, or insufficient adjustment for clinical confounders.[7,8]

To address these limitations, opportunistic computed tomography (CT) phenotyping has emerged as a scalable strategy for extracting quantitative biomarkers from routinely acquired imaging without additional scans or radiation exposure.[10] While cross-sectional skeletal muscle area at the third lumbar vertebra (L3) remains the conventional reference standard,[11] abdominal imaging is not routinely available in many HNC workflows. As a result, studies have validated single-slice tissue measurements at the third cervical vertebra (C3) as a surrogate.[12,13] These studies demonstrated that reduced skeletal muscle and elevated intermuscular adiposity are associated with frailty, impaired treatment tolerance, and inferior oncologic outcomes.[14-17] In particular, increasing attention has focused on myosteatosis and intermuscular adipose infiltration as imaging biomarkers of impaired muscle quality, systemic inflammation, metabolic dysfunction, and cancer-associated frailty.[18] Together, body composition phenotype and muscle quality may provide meaningful prognostic information.

Despite growing interest in body composition analysis, most prior approaches have relied on manually derived single-slice measurements that are labor intensive, susceptible to interobserver variability, and difficult to scale clinically.[19,20] More recent studies have explored deep learning–assisted automation of cervical muscle segmentation and sarcopenia assessment in HNC.[21,22] However, many existing approaches remain focused on single-slice muscle measurements rather than an automated volumetric phenotyping of multiple soft tissue compartments integrated within routine RT imaging workflows. Volumetric analysis may better capture soft tissue heterogeneity while remaining compatible with scalable clinical deployment. More broadly, recent advances in deep learning–based body composition analysis have demonstrated the feasibility of automated multicomponent volumetric phenotyping from routine CT imaging.[23] We sought to address how baseline body composition metrics provide biological granularity into physiological reserve and are associated with OS in patients with HNC.

Key Points

Question How do baseline body composition metrics provide biological granularity into physiologic reserve and how are they associated with overall survival in patients with head and neck cancer?

Findings In this cohort study of 1187 patients with head and neck cancer, an elevated body mass index was associated with improved survival. An automated volumetric analysis of an imaging subcohort (n = 659) demonstrated that higher skeletal muscle and lower intermuscular adiposity were independently associated with favorable outcomes.

Meaning The study results suggest that while elevated body mass index categories are associated with overall survival, automated soft tissue phenotyping further investigates underlying physiologic reserve, allowing clinicians to risk-stratify patients based on body composition analyses for individualized supportive care during oncologic treatment.

Objective

In this study, we developed an automated, deep learning–based pipeline to quantify 3-dimensional (3D) cervical neck soft tissue volumes from routine pretreatment CT simulation scans in a large cohort of patients undergoing RT for HNC. Using an open source autosegmentation framework, we extracted volumetric measures of skeletal muscle, subcutaneous adipose tissue, and intermuscular adipose tissue to derive imaging-based biomarkers of body composition and host vulnerability.[24] We evaluated the prognostic use of conventional BMI stratification and our volumetric biomarkers with respect to an established set of clinical risk factors. To our knowledge, this was the first automated, deep learning–driven, multicompartment 3D body composition phenotyping performed at an institutional scale in HNC. By leveraging opportunistic CT imaging, this framework revealed novel biological granularity, motivating the integration of imaging-derived biomarkers into radiation oncology workflows for pretreatment risk stratification.

Methods

Patient Selection

We conducted a retrospective cohort study that integrated computational imaging biomarkers, electronic health record (EHR) data, RT planning data, and CT imaging data from patients who were treated with definitive RT for HNC at our institution (University of California, Los Angeles) and treated with conventional C-arm linear accelerators between January 1, 2014, and December 31, 2024. This study received approval from the

© 2026 American Medical Association. All rights reserved, including those for text and data mining, AI training, and similar technologies.

Downloaded from jamanetwork.com by University of California - Los Angeles user on 10/08/2026

institutional review board at our institution, which waived consent due to the retrospective nature of the study. The study followed the Strengthening the Reporting of Observational Studies in Epidemiology (STROBE) reporting guideline.

Patients were identified through the institutional data warehouse using HNC *International Classification of Diseases, Ninth Revision (ICD-9)* and *International Statistical Classification of Diseases and Related Health Problems, Tenth Revision (ICD-10)* codes recorded during the study period. Inclusion criteria required patients to have undergone definitive-intent RT. Exclusion criteria included a treatment course of fewer than 20 fractions or an unapproved Digital Imaging and Communications in Medicine RT plan. These thresholds were selected to preferentially capture conventionally fractionated, definitive-intent RT courses while excluding palliative, abbreviated, or nonstandard treatment regimens.

EHR Data Collection

EHR data were extracted from the institutional clinical data warehouse. eMethods 1 in Supplement 1 further describes the methods.

Imaging Data Extraction

Pretreatment CT simulation imaging results were available for a subset of the cohort and used for the body composition analysis. These scans are routinely acquired before RT initiation for treatment positioning and RT dose planning; therefore, they provide an opportunistic imaging source for body composition phenotyping without additional imaging acquisition.

Patients whose imaging data could not be retrieved from the institutional picture archiving and communication system were excluded. To ensure the availability of longitudinal treatment imaging and confirm standard definitive-intent treatment workflows, patients were additionally required to have at least 20 daily treatment imaging datasets accessible within the treatment record. Patients treated on ring-gantry linear accelerator platforms lacking cone beam CT-based image guidance were excluded, including TomoTherapy (Accuray Inc) and MRIdian Linac (ViewRay Inc).

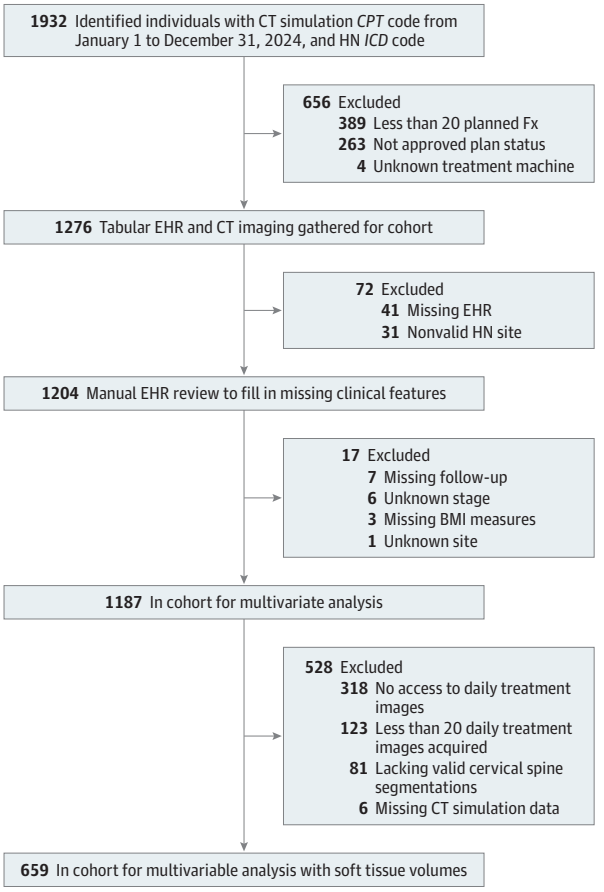
Image Processing

Pretreatment CT simulation scans underwent automated segmentation using TotalSegmentator, an open source, deep learning-based framework for anatomical segmentation.[24] The "total," "body," and "tissue_4_types" subtasks were used to delineate total body volume, soft tissue compartments (skeletal muscle, subcutaneous adipose tissue, and intermuscular adipose tissue), and vertebral bodies. The overall computational workflow for automated image processing, extraction of volumetric body composition metrics, and downstream prognostic modeling is summarized in eFigure 1 in Supplement 1, and details regarding methods are outlined in eMethods 2 in Supplement 1.

Cinematic Rendering

Soft tissue compartments and tumor volume were visualized through a 3D cinematic rendering generated using ParaView (version 6.1.0; Kitware Inc). eMethods 3 in Supplement 1 further describes the methods.

Figure 1. Patient Selection Flowchart



Strengthening the Reporting of Observational Studies in Epidemiology diagram illustrating cohort assembly and exclusion criteria for the retrospective head and neck (HN) cancer study population. The final clinical cohort included 1187 patients, of whom 659 received pretreatment computed tomography (CT) simulation imaging suitable for volumetric body composition analysis. BMI indicates body mass index; *CPT*, *Current Procedural Terminology*; EHR, electronic health record; Fx, fraction; *ICD*, *International Classification of Diseases*.

Statistical Analysis

Summary statistics of clinical features were presented in a table using the *tableone* (version 0.9.5) Python package. OS was defined as the primary clinical end point and calculated from the date of CT simulation to the date of death of any cause, with surviving patients censored at the date of last clinical follow-up.

To evaluate the independent prognostic significance of baseline clinical variables, multivariable Cox proportional hazards regression models were constructed. Confounding variables were selected from literature-based, established prognostic factors in HNC. Model adequacy was verified by confirming an events-per-variable ratio of 24.75 for the clinical cohort and 11.47 for the smaller imaging subcohort. Multicollinearity among covariates was assessed using variance inflation factor testing implemented through the *statsmodels* (version 0.14.6) Python package. To preserve model stability, categorical variables with sparse frequencies were consolidated into broader, clinically meaningful groupings.

© 2026 American Medical Association. All rights reserved, including those for text and data mining, AI training, and similar technologies.

Downloaded from jamanetwork.com by University of California - Los Angeles user on 10/08/2026

Table. Baseline Demographic and Clinical Characteristics of 1187 Patients Treated With Head and Neck Radiotherapy

Characteristic	Overall, No. (%)
Age, median (range), y[a]	64.0 (5.0-100.0)
Sex	
Female	323 (27.2)
Male	864 (72.8)
BMI, median (range)	25.5 (12.9-62.0)
BMI category	
Underweight (<18.5)	39 (3.3)
Healthy (18.5-24.9)	500 (42.1)
Overweight (25-29.9)	421 (35.5)
Obesity (≥30)	227 (19.1)
Smoking status	
Heavy (≥10 pack-year)	176 (14.8)
Moderate (<10 pack-year)	95 (8.0)
Never smoker	678 (57.1)
Unknown	238 (20.1)
ECOG PS[b]	
0: Fully active	631 (53.2)
1: Restricted activity	467 (39.3)
≥2 (2/3/4)	89 (7.5)
2: Ambulatory/self-care	59 (5.0)
3: Limited self-care	25 (2.1)
4: Completely disability	5 (0.4)
Primary tumor site	
Larynx/hypopharynx	126 (10.6)
Nasopharynx/sinus	126 (10.6)
Oral cavity	270 (22.7)
Oropharynx	461 (38.8)
Skin/salivary/thyroid	204 (17.2)
Disease stage[c]	
0/I	236 (19.9)
0	5 (0.4)
I	231 (19.4)
II	259 (21.8)
III	265 (22.3)
IV	427 (36.0)
HPV status	
HPV-positive OPC	367 (30.9)
HPV-negative OPC	71 (6.0)
Non-OPC NA	749 (63.1)
Treatment modality	
Definitive RT	574 (48.4)
Surgery + adjuvant RT	613 (51.6)
Chemotherapy regimen[b]	
Concurrent	461 (38.8)
Concurrent + adjuvant	7 (0.6)
Concurrent only	396 (33.4)
Induction + concurrent	58 (4.9)
None/induction/salvage	726 (61.2)
Induction only	36 (3.0)
No systemic therapy	578 (48.7)
Salvage chemotherapy only	112 (9.4)

Abbreviations: BMI, body mass index (calculated as weight in kilograms divided by height in meters squared); ECOG PS, Eastern Cooperative Oncology Group performance status; HPV, human papillomavirus; NA, not applicable; OPC, oropharyngeal cancer; RT, radiotherapy; sex, sex assigned at birth.

[a] The minimum age of 5 years reflects a small subset of pediatric cases (n = 6) included in the cohort, comprising diagnoses of rhabdomyosarcoma, mucoepidermoid carcinoma, and scalp sarcoma.

[b] Percentages for indented variables represent their proportion of the total cohort (N = 1187) and are provided as a detailed breakdown of the broader category they are within, which is used for multivariable modeling.

[c] Disease stage reflects *American Joint Committee on Cancer Staging Manual, 8th Edition* staging.

Kaplan-Meier survival curves were generated for variables demonstrating statistical significance within multivariable analysis. Differences in survival distributions between groups were assessed using the log-rank test. For variables containing more than 2 categories, pairwise post hoc log-rank testing was performed, with *P* values adjusted for multiple comparisons using the Bonferroni correction.

A second multivariable Cox regression model was subsequently constructed within the imaging subcohort to evaluate imaging-derived body composition biomarkers, namely skeletal muscle index (SMI) and intermuscular adiposity index (IAI) scores. A Pearson bivariate correlation analysis was performed to assess redundancy and collinearity among tissue variables.

To visualize the independent prognostic associations of body composition biomarkers, covariate-adjusted survival curves were generated from the fitted Cox regression model. Partial effect plots were created to isolate hazard trajectories associated with SMI and IAI on OS. Expected survival probabilities were estimated for hypothetical patient profiles representing low (−1 SD), mean (0 SD), and high (1 SD) tissue index distributions while holding all remaining covariates constant at reference values.

Comparative prognostic models included a clinical baseline model (CBM), CBM with BMI, CBM with soft tissue indices, and a combined model that integrated all features. Model discrimination was evaluated using the Harrell concordance index (C-index). 95% CIs for C-indices were estimated using 500 bootstrap iterations of the paired predicted partial hazards and observed survival outcomes from the primary models. Nested Cox model comparisons were assessed using likelihood ratio testing to evaluate the incremental prognostic contribution of BMI and imaging-derived body composition biomarkers in addition to conventional clinical variables. A decision curve analysis estimated the relative net clinical benefit across threshold probabilities using predicted survival probabilities. While BMI was excluded from the primary hazard ratio (HR) estimations to prevent coefficient destabilization due to multicollinearity, it was integrated in the discrimination analysis to evaluate the incremental prognostic use of the imaging metrics beyond BMI.

© 2026 American Medical Association. All rights reserved, including those for text and data mining, AI training, and similar technologies.

Downloaded from jamanetwork.com by University of California - Los Angeles user on 10/08/2026

Statistical analyses were performed using Python (version 3.11.14) with the *dcurves* (version 1.1.7) and *lifelines* (0.30.0) packages.[25,26] Statistical significance was defined as 2-sided $P < .05$. To distinguish statistical significance from clinical relevance, an HR magnitude of 0.80 or less (for protective factors) or 1.25 or greater (for risk factors) was established a priori as the threshold for a minimal clinically important difference based on established oncology frameworks.[27]

Results

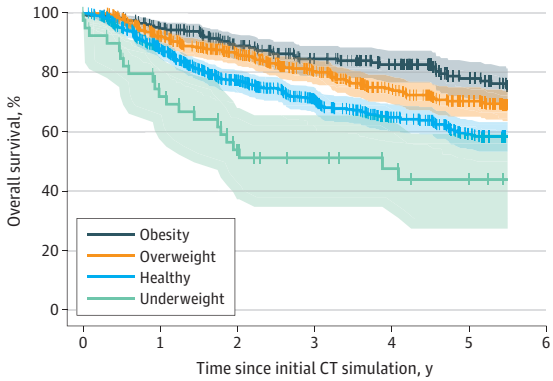
A total of 1276 patients treated with definitive-intent RT for HNC between January 1, 2014, and December 31, 2024, were identified through the institutional clinical and RT databases. Following EHR harmonization and quality filtering, complete clinical data were available for 1187 patients (median [range] age, 64.0 [5.0-100.0] years; 323 female individuals [27.2%] and 864 male individuals [72.8%]), comprising the primary cohort for the multivariable analysis. Among these, pretreatment CT simulation imaging scans that were suitable for automated volumetric body composition analysis were available for 659 patients (**Figure 1).** Baseline demographic, clinical, and treatment characteristics are summarized in the **Table**. At the time of analysis, 396 deaths had occurred. Using the reverse Kaplan-Meier method, the median follow-up time was 5.5 years (IQR, 3.0-8.2). The estimated median OS for the cohort was 10.9 years (IQR, 3.1 to not reached).

Clinical Cohort Survival Analysis

Kaplan-Meier analysis demonstrated unadjusted OS differences across baseline BMI categories (**Figure 2**). Specifically, patients with overweight (univariate HR, 0.62; 95% CI, 0.50-0.77) and obesity (univariate HR, 0.51; 95% CI, 0.38-0.69) exhibited prolonged survival compared with patients with a healthy BMI (pairwise adjusted log-rank $P = .001$ and $P < .001$, respectively). Kaplan-Meier curves for additional baseline covariates are provided in eFigures 6 to 11 in Supplement 1.

To determine whether these survival differences persisted after adjustment for baseline confounders, a multivariable Cox proportional hazards regression was performed within the full clinical cohort (N = 1187). Because of the multicollinearity between human papillomavirus (HPV) status and oropharyngeal cancer (OPC) primary site, a composite categorical variable was constructed to stratify patients into HPV-positive OPC, HPV-negative OPC, and non-OPC groups. Advanced age, impaired performance status, and higher disease stage were independently associated with inferior survival (**Figure 3**). Treatment year was included as a covariate to account for temporal differences. While the point estimate suggested a 3% decrease in the relative risk of death for each subsequent year of treatment, this variable did not demonstrate a clear association with OS (HR, 0.97; 95% CI, 0.93-1.01; $P = .09$). Elevated baseline BMI remained independently associated with improved survival. Compared with patients with a healthy BMI, patients with overweight (HR, 0.70; 95% CI, 0.56-0.89; $P = .004$) and obesity (HR, 0.67; 95% CI, 0.50-0.91; $P = .01$) demonstrated reduced mortality risk.

Figure 2. Kaplan-Meier Survival Curve Showing Overall Survival as Stratified by Baseline Body Mass Index Category for 1187 Participants



No. at risk (censored)

Obesity	227 (0)	213 (4)	176 (29)	144 (52)	124 (69)	98 (90)
Overweight	421 (0)	371 (18)	312 (54)	253 (93)	203 (126)	164 (154)
Healthy	500 (0)	427 (14)	337 (54)	266 (99)	205 (139)	160 (168)
Underweight	39 (0)	30 (0)	22 (0)	18 (3)	15 (6)	12 (7)

Pairwise adjusted log-rank values for groups with overweight and obesity compared with healthy individuals were .001 and >.001, respectively. Time 0 corresponds to the date of computed tomography (CT) simulation. Shaded regions represent 95% CIs.

Automated Volumetric Body Composition Analysis

Automated volumetric segmentation enabled quantitative phenotyping of cervical neck skeletal muscle, subcutaneous adipose tissue, and intermuscular adipose tissue compartments from routine CT simulation imaging. Representative 3D cinematic renderings of segmental tissue compartments and the treatment target volume are shown in eFigure 12 in Supplement 1 for a sample patient. Summary clinical characteristics and statistics for the imaging subcohort (n = 659) are provided in eTable 1 in Supplement 1, while raw tissue volumes and derived indices are listed in eTable 2 in Supplement 1.

Volumetric tissue composition analysis demonstrated substantial heterogeneity across BMI strata (eFigure 13 in Supplement 1). Normalized total tissue volume increased approximately 3.5-fold from the underweight to obese BMI categories. However, this expansion primarily consisted of subcutaneous adipose tissue rather than skeletal muscle preservation. The relative proportion of subcutaneous adipose tissue was higher across increasing BMI categories, ranging from 27% in underweight patients to 48% in patients with obesity. These findings highlight the potential limitations of using BMI as a surrogate for physiologic reserve and body composition phenotyping. Additional comparisons between volumetric body composition metrics and BMI are provided in eFigures 14 to 15 in Supplement 1.

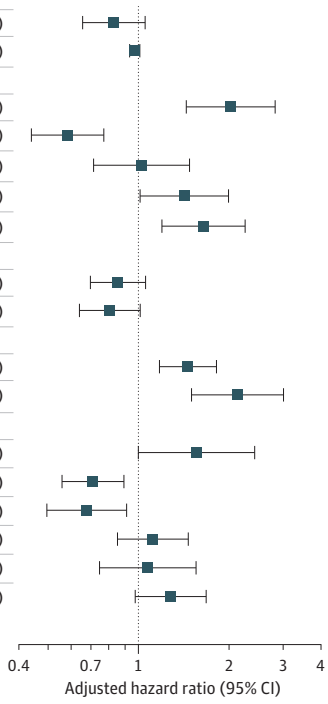
Imaging-Derived Biomarkers and Survival

Within the imaging subcohort, a second multivariable Cox proportional hazards model evaluated the independent prognostic significance of imaging-derived body composition biomarkers (**Figure 4**). BMI was excluded from this multivariable model because of the collinearity with the imaging-derived body composition metrics. Additionally, substantial collinearity be-

© 2026 American Medical Association. All rights reserved, including those for text and data mining, AI training, and similar technologies.
Downloaded from jamanetwork.com by University of California - Los Angeles user on 10/08/2026

Figure 3. Dot Plot of Results of a Multivariable Cox Regression for 1187 Participants

	Adjusted hazard ratio (95% CI)
Demographics and temporal	
Female vs male	0.83 (0.65-1.05)
Treatment year	0.97 (0.93-1.01)
Tumor characteristics	
HPV- OPC vs non-OPC	2.01 (1.43-2.82)
HPV+ OPC vs non-OPC	0.58 (0.44-0.76)
Stage II vs 0-I	1.02 (0.71-1.47)
Stage III vs 0-I	1.41 (1.01-1.98)
Stage IV vs 0-I	1.63 (1.19-2.24)
Treatment	
Surgery + adjuvant RT vs definitive RT	0.85 (0.69-1.05)
Concurrent chemotherapy	0.80 (0.63-1.01)
Performance status	
ECOG 1 vs 0	1.45 (1.17-1.80)
ECOG 2-4 vs 0	2.12 (1.49-3.01)
Lifestyle and comorbidities	
Underweight vs healthy BMI	1.55 (0.99-2.41)
Overweight vs healthy BMI	0.70 (0.56-0.89)
Obesity vs healthy BMI	0.67 (0.50-0.91)
Unknown vs never smoker	1.11 (0.85-1.45)
Moderate smoking (<10 PY) vs never smoker	1.07 (0.74-1.54)
Heavy smoking (≥10 PY) vs never smoker	1.27 (0.97-1.67)



Reference groups were individuals who were male, had a healthy body mass index (BMI), never smoked, had an Eastern Cooperative Oncology Group (ECOG) score of 0, did not have oropharyngeal cancer (OPC), had stage 0 to I disease, received definitive radiotherapy (RT), and did not receive systemic therapy. Age was adjusted for as a continuous variable, and treatment year was a continuous, 0-anchored covariate. Points represent hazard ratios, and error bars indicate the 95% CIs. HPV indicates human papillomavirus; HPV−, HPV negative; HPV+, HPV-positive; PY, pack-years.

tween the subcutaneous adiposity index and IAI prompted inclusion of only the IAI and SMI in the model.

A higher SMI score was independently associated with OS, with each 1-SD increase associated with a 33% reduction in the mortality hazard (HR, 0.67; 95% CI, 0.50-0.89; $P = .001$). Conversely, elevated IAI scores were independently associated with inferior OS, with each 1-SD increase associated with a 28% increase in the mortality hazard (HR, 1.28; 95% CI, 1.03-1.58; $P = .02$).

Covariate-adjusted survival curves were generated to visualize these longitudinal effects. Consistent with the multivariable Cox regression, the models demonstrated divergent survival trajectories according to tissue composition phenotypes (eFigure 16 in Supplement 1). Higher SMI remained associated with improved OS over time, whereas elevated IAI scores corresponded to progressively worse survival outcomes across standardized tissue distributions.

Incremental Prognostic Use of Imaging Biomarkers

To evaluate the incremental prognostic use, discrimination performance was assessed across 4 nested models: CBM, CBM + BMI, CBM + tissue indices, and a combined model that integrated BMI and imaging-derived tissue biomarkers. The CBM demonstrated a C-index of 0.714 (95% CI, 0.679-0.750), with only minimal improvement following BMI incorporation alone (C-index, 0.716; 95% CI, 0.679-0.755). Adding imaging-derived tissue biomarkers improved discrimination to 0.725 (95% CI, 0.689-0.759), whereas the combined model achieved the highest performance at 0.733 (95% CI, 0.697-0.768) (eTable 3 in Supplement 1).

Likelihood ratio testing demonstrated incremental prognostic value associated with imaging-derived tissue biomarkers beyond clinical variables and BMI ($\chi^2 = 14.55$). A decision curve analysis compared the clinical benefit of the survival models for 5-year OS prediction (eFigure 17 in Supplement 1).

Discussion

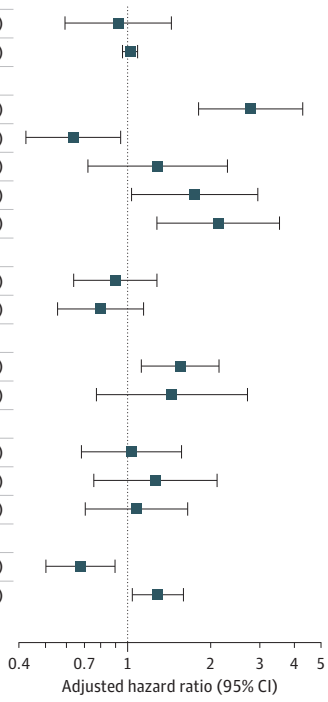
In this cohort study, we analyzed multiple body composition metrics acquired for patients with HNC before initiating RT. First, in more than 1100 patients, we found that elevated baseline BMI was independently associated with improved OS, reflecting the commonly described obesity paradox in HNC and other cancers.[4,7,8] To our knowledge, this is the largest study to date that examined BMI in all 4 classes from underweight to obesity, showing marked separation in the Kaplan-Meier curves for each group. These data suggest that higher baseline body mass is independently associated with improved OS following RT for HNC.

However, BMI incompletely captures body composition heterogeneity and may partially reflect preserved physiologic reserve rather than adiposity itself. Prior obesity literature has additionally been influenced by smoking-related confounding, reverse causality from cachexia, and baseline frailty.[4,6] Our volumetric analyses further demonstrated that increasing BMI disproportionately reflected subcutaneous adipose tissue expansion rather than preservation of

© 2026 American Medical Association. All rights reserved, including those for text and data mining, AI training, and similar technologies.
Downloaded from jamanetwork.com by University of California - Los Angeles user on 10/08/2026

Figure 4. Dot Plot of Results of a Multivariate Cox Regression for 659 Participants

	Adjusted hazard ratio (95% CI)
Demographics and temporal	
Female vs male	0.92 (0.59-1.43)
Treatment year	1.01 (0.95-1.08)
Tumor characteristics	
HPV- OPC vs non-OPC	2.78 (1.80-4.29)
HPV+ OPC vs non-OPC	0.63 (0.42-0.94)
Stage II vs 0-I	1.28 (0.71-2.29)
Stage III vs 0-I	1.74 (1.03-2.95)
Stage IV vs 0-I	2.12 (1.27-3.53)
Treatment	
Surgery + adjuvant RT vs definitive RT	0.90 (0.63-1.27)
Concurrent chemotherapy	0.79 (0.55-1.13)
Performance status	
ECOG 1 vs 0	1.54 (1.11-2.13)
ECOG 2-4 vs 0	1.44 (0.76-2.70)
Lifestyle	
Unknown vs never smoker	1.03 (0.67-1.56)
Moderate smoking (<10 PY) vs never smoker	1.25 (0.75-2.10)
Heavy smoking (≥10 PY) vs never smoker	1.07 (0.70-1.64)
Body composition	
Skeletal muscle index	0.67 (0.50-0.89)
Intermuscular fat index	1.28 (1.03-1.58)



Body composition biomarkers were modeled as continuous standardized variables. Reference groups for the categorical variables were individuals who were male, had a healthy body mass index (BMI), never smoked, had an Eastern Cooperative Oncology Group (ECOG) score of 0, did not have oropharyngeal cancer (OPC), had stage 0 to I disease, received definitive radiotherapy (RT), and did not receive systemic therapy. Age was adjusted for as a continuous variable, and treatment year was a continuous, 0-anchored covariate. Points represent hazard ratios, and error bars indicate 95% CIs. HPV indicates human papillomavirus; HPV−, HPV negative; HPV+, HPV-positive; PY, pack-years.

skeletal muscle, emphasizing the potential limitations of BMI as a surrogate for treatment resilience during RT.

We developed an automated, deep learning–based pipeline to extract quantitative 3D soft tissue metrics using standard pretreatment CT imaging in patients undergoing RT for HNC. To our knowledge, this was the first automated, multicompartment 3D body composition phenotyping conducted at an institutional scale using routinely collected imaging. While we confirmed that higher baseline BMI is associated with improved OS, we also demonstrated that gross BMI can mask divergent physiological risks. An analysis of volumetric soft tissue indices revealed that higher SMI scores are associated with improved survival, whereas elevated IAI scores are associated with an increased risk of mortality. Combining these imaging-derived body composition metrics with standard clinical variables and BMI yielded an improvement in prognostic model fit. Ultimately, this scalable pipeline demonstrates the use of integrating opportunistic imaging biomarkers into routine risk stratification. Future prospective studies are warranted to determine if identifying these vulnerable patient profiles before treatment can effectively guide personalized nutritional and therapeutic interventions.

The study's automated 3D metrics aligned with growing literature implicating myosteatosis and intermuscular adipose infiltration as imaging biomarkers of impaired muscle quality, systemic inflammation, metabolic dysfunction, and frailty.[17,18] Therefore, high IAI scores may flag a biologic vulnerability that is not captured by BMI alone, suggesting that soft tissue distribution could provide an improved characterization of host resilience during RT compared with gross body weight.

Strength and Limitations

This study had several strengths, including the integration of large-scale EHR, RT planning, and imaging datasets within a clinically used radiation oncology environment. Additionally, the use of an automated pipeline enabled the scalable, simultaneous assessment of multiple cervical neck tissue compartments as opposed to conventional single-slice approaches that rely on manual contouring.[12,13,16,20] These findings further support the broader role of opportunistic imaging phenotyping and computational biomarker extraction from routinely acquired clinical datasets.[10]

Because CT simulation scans are routinely obtained before RT initiation, automated body composition phenotyping may enable pretreatment risk stratification without additional image acquisition or clinical burden. Integrating these biomarkers into existing radiation oncology workflows may facilitate earlier identification of patients with highly vulnerable prognostic profiles. Flagging these high-risk cohorts is a critical step toward evaluating whether they might benefit from intensified supportive care, including nutritional assessment, exercise oncology referral, adaptive monitoring, or multidisciplinary intervention.[28] Although pharmacologic interventions targeting cachexia-associated muscle loss remain investigational,[29,30] future prospective studies are needed to determine whether body composition–guided interventions improve clinical outcomes.

© 2026 American Medical Association. All rights reserved, including those for text and data mining, AI training, and similar technologies.

Downloaded from jamanetwork.com by University of California - Los Angeles user on 10/08/2026

Several limitations should also be acknowledged. Automated segmentation was performed using TotalSegmentator, a deep learning framework that is primarily trained on nonpathologic anatomy.[24] Consequently, segmentation accuracy may be reduced in patients with substantial anatomic distortion from bulky primary tumors or nodal disease. Although potential segmentation errors were minimized through cohort filtering steps, vertebral completeness criteria, tumor volume subtraction, and manual quality assurance review, formal expert contour validation and intermethod benchmarking were not performed. Further, the training dataset (including training, validation, and test sets) comprised randomly sampled CT images from routine clinical studies, ensuring a clinical dataset that explicitly included head and neck studies.[24] In addition, the imaging subcohort represented a subset of the broader clinical cohort because of scan availability and treatment platform constraints. While this retrospective filtering could potentially introduce selection bias, baseline demographic and clinical characteristics remained broadly comparable between cohorts (eTable 1 in Supplement 1). As a more formal comparison, we conducted a multivariable Cox regression sensitivity analysis with subcohort inclusion as an independent variable. We found that subcohort inclusion was not independently associated with OS (adjusted HR, 0.84; 95% CI, 0.68-1.04; P = .11; eMethods 4 and eTables 4 and 5 in Supplement 1). Furthermore, the HRs reported in our models reflect weak associations according to the classification magnitude proposed by Grimes and Schulz[31] (weak: 1.0-3.9; moderate: 4.0-7.9; strong: ≥8.0). A caveat to our findings is that they could be susceptible to confounding or bias, warranting cautious clinical interpretation. Some specific unmeasured variables were precise smoking history and systemic therapy that did not include chemotherapy, representing potential sources of residual confounding that were not accounted for in this retrospective dataset. Finally, external validation across independent institutions and diverse imaging workflows will also be necessary before broader clinical deployment.

The use of OS as the primary end point warrants additional consideration because body composition biomarkers may reflect broader physiologic health, frailty, cardiovascular risk, and noncancer mortality in addition to cancer-specific treatment tolerance. Future studies incorporating treatment-related toxic effects, feeding tube dependence, hospitalization, treatment interruptions, and longitudinal body composition trajectories may provide further biologic and clinical insight. Oncologic end points such as progression-free survival and locoregional control are highly valuable, but often require extensive manual curation. Feeding tube dependence has limitations in broader applicability, as the institutional placement rates vary drastically from as low as 15% to more than 70%.[32,33] This is largely associated with differing clinical cultures between academic centers and community clinics, as well as institutional preferences for prophylactic vs reactive placement. A particularly exciting area of active investigation for our group involves repurposing daily setup images (cone beam CT) acquired during RT to objectively track longitudinal changes in soft tissue composition.

Although to our knowledge this was the largest study to date that examined BMI in all 4 classes from underweight to obese, the wide CIs in the small underweight cohort (n = 39) necessitate cautious interpretation of this specific subgroup. Further, while integrating automated 3D body composition metrics provided an improvement in model discrimination, we acknowledge that the absolute incremental gain over the clinical baseline model was modest (C-index increase of 0.019). This delta highlights the established, dominant prognostic weight of conventional clinical variables for this oncologic population. Ultimately, prospective validation will be essential in translating these imaging-derived body composition biomarkers into clinical tools that guide precision risk stratification and personalize supportive care for patients undergoing RT for HNC.

A recent study[34] that investigated pretreatment BMI and 3D body composition metrics in a HNC cohort found that BMI was not significantly associated with OS. Several key differences likely contributed to this finding. First, their analysis relied on a smaller cohort (N = 391) that was limited exclusively to patients with surgically treated head and neck squamous cell carcinoma, contrasting with our broader, RT-focused HNC cohort. Second, they evaluated BMI using a median split, whereas our analysis assessed survival differences across the 4 clinical BMI categories. Despite these variations, both studies support a unified conclusion that volumetric body composition may provide additional information beyond BMI alone. They demonstrated that a higher cervical sarcopenia index was associated with improved survival. Ultimately, despite the nondefinitive BMI findings, both studies suggest that BMI and volumetric body composition metrics capture association but distinct biological information.

Conclusions

This cohort study analyzed multiple body composition metrics for more than 1100 patients with HNC before RT, representing what is to our knowledge the largest single-institutional analysis of this population to date. An elevated baseline BMI was independently associated with improved OS, which was consistent with a survival advantage among patients with higher body mass. Further, conducting an automated 3D body composition analysis using routine pretreatment CT simulation scans enabled volumetric phenotyping at scale, revealing that specific soft tissue compartments are associated with divergent survival outcomes. Higher skeletal muscle compared with height was associated with favorable survival outcomes, while higher intermuscular adiposity compared with height was associated with poorer overall survival. By providing this biological granularity, our framework introduced a robust method of extracting soft tissue indices to guide prognostication. Ultimately, integrating this opportunistic phenotyping into clinical infrastructure may refine baseline risk stratification, providing critical prognostic context to help flag vulnerable patients for future prospective trials that evaluate targeted supportive care to endure cancer-directed therapy.

© 2026 American Medical Association. All rights reserved, including those for text and data mining, AI training, and similar technologies.

Downloaded from jamanetwork.com by University of California - Los Angeles user on 10/08/2026

ARTICLE INFORMATION

Accepted for Publication: August 16, 2026.

Published Online: October 8, 2026. doi:10.1001/jamaoto.2026.2951

Author Contributions: Ms Jank had full access to all of the data in the study and takes responsibility for the integrity of the data and the accuracy of the data analysis. Ms Jank and Dr Bang were co–first authors, and Drs Sung and Savjani were co–senior authors.
Concept and design: Jank, Bang, Gillett, Sung, Savjani.
Acquisition, analysis, or interpretation of data: Jank, Bang, Raj, Villafuerte, Oh, Militchin, Chau, Qi, Chin, Savjani.
Drafting of the manuscript: Jank, Bang, Militchin, Sung, Savjani.
Critical review of the manuscript for important intellectual content: Jank, Bang, Raj, Gillett, Villafuerte, Oh, Militchin, Chau, Qi, Chin, Savjani.
Statistical analysis: Jank, Bang, Oh, Savjani.
Obtained funding: Jank, Savjani.
Administrative, technical, or material support: Jank, Bang, Raj, Militchin, Qi, Chin, Sung, Savjani.
Supervision: Jank, Raj, Sung, Savjani.

Conflict of Interest Disclosures: Dr Sung reported grants from Siemens Healthineers outside the submitted work. Dr Savjani reported grants from StratPharma, BrainLab, and the Radiation Oncology Institute and personal fees from Varian outside the submitted work. No other disclosures were reported.

Funding/Support: This study was partially supported by a grant from the Jonsson Comprehensive Cancer Center at the University of California, Los Angeles.

Role of the Funder/Sponsor: The funding organizations had no role in the design and conduct of the study; collection, management, analysis, and interpretation of the data; preparation, review, or approval of the manuscript; and decision to submit the manuscript for publication.

Data Sharing Statement: See Supplement 2.

Additional Contributions: We acknowledge Nicholas Jackson, PhD, University of California, Los Angeles (UCLA), for his expert review and guidance with the statistical methods and Varun Badheka, MS, UCLA, for his technical expertise in exploring the 3-dimensional cinematic rendering techniques during the development of this manuscript. Neither of these individuals were compensated for their contributions.

REFERENCES

1. Anderson G, Ebadi M, Vo K, Novak J, Govindarajan A, Amini A. An updated review on head and neck cancer treatment with radiation therapy. *Cancers (Basel)*. 2021;13(19):4912. doi:10.3390/cancers13194912
2. Powrózek T, Dziwota J, Małecka-Massalska T. Nutritional deficiencies in radiotherapy-treated head and neck cancer patients. *J Clin Med*. 2021;10(4):574. doi:10.3390/jcm10040574
3. Bozzetti F, Cotogni P. Nutritional issues in head and neck cancer patients. *Healthcare (Basel)*. 2020;8(2):102. doi:10.3390/healthcare8020102
4. Fearon K, Strasser F, Anker SD, et al. Definition and classification of cancer cachexia: an international consensus. *Lancet Oncol*. 2011;12(5):489-495. doi:10.1016/S1470-2045(10)70218-7
5. Rozynek M, Gut D, Kucybała I, et al. Fully automated 3D body composition analysis and its association with overall survival in head and neck squamous cell carcinoma patients. *Front Oncol*. 2023;13:1176425. doi:10.3389/fonc.2023.1176425
6. Meerkerk CDA, Chargi N, de Jong PA, van den Bos F, de Bree R. Low skeletal muscle mass predicts frailty in elderly head and neck cancer patients. *Eur Arch Otorhinolaryngol*. 2022;279(2):967-977. doi:10.1007/s00405-021-06835-0
7. Ma SJ, Khan M, Chatterjee U, et al. Association of body mass index with outcomes among patients with head and neck cancer treated with chemoradiotherapy. *JAMA Netw Open*. 2023;6(6):e2320513. doi:10.1001/jamanetworkopen.2023.20513
8. Pastorino R, Pires Marafon D, Lentini N, et al. The effect of body mass index at diagnosis on survival of patients with squamous cell head and neck carcinoma. *Am J Cancer Res*. 2024;14(11):5411-5426. doi:10.62347/UUXK7608
9. Vangelov B, Smee RI, Bauer J. Sarcopenic obesity in patients with head and neck cancer is predictive of critical weight loss during radiotherapy. *Br J Nutr*. 2024;132(5):599-606. doi:10.1017/S0007114524001880
10. Pickhardt PJ. Value-added opportunistic CT screening: state of the art. *Radiology*. 2022;303(2):241-254. doi:10.1148/radiol.211561
11. Rinninella E, Cintoni M, Raoul P, et al. Muscle mass, assessed at diagnosis by L3-CT scan as a prognostic marker of clinical outcomes in patients with gastric cancer: a systematic review and meta-analysis. *Clin Nutr*. 2020;39(7):2045-2054. doi:10.1016/j.clnu.2019.10.021
12. Pisani C, Mastroleo F, Collo A, et al. Variation in body mass and skeletal muscle indices in head and neck cancer patients undergoing (chemo) radiotherapy and nutritional intervention. *Curr Oncol*. 2022;30(1):250-260. doi:10.3390/curroncol30010020
13. Miola TM, Bitencourt AGV, Souza JO, Kowalski LP, Gonçalves Filho J. Analysis of muscle mass by computed tomography in patients with head and neck cancer: a prospective study. *Radiol Bras*. 2023;56(5):269-274. doi:10.1590/0100-3984.2023.0037
14. Takenaka Y, Takemoto N, Otsuka T, et al. Predictive significance of body composition indices in patients with head and neck squamous cell carcinoma treated with nivolumab: a multicenter retrospective study. *Oral Oncol*. 2022;132:106018. doi:10.1016/j.oraloncology.2022.106018
15. Carrilho LAO, Juliani FL, Moreira RCL, et al. Adipose tissue characteristics as a new prognosis marker of patients with locally advanced head and neck cancer. *Front Nutr*. 2025;12:1472634. doi:10.3389/fnut.2025.1472634
16. Thureau S, Lebret L, Lequesne J, et al. Prospective evaluation of sarcopenia in head and neck cancer patients treated with radiotherapy or radiochemotherapy. *Cancers (Basel)*. 2021;13(4):753. doi:10.3390/cancers13040753
17. Bardoscia L, Besutti G, Pellegrini M, et al. Impact of low skeletal muscle mass and quality on clinical outcomes in patients with head and neck cancer undergoing (chemo)radiation. *Front Nutr*. 2022;9:994499. doi:10.3389/fnut.2022.994499
18. Aubrey J, Esfandiari N, Baracos VE, et al. Measurement of skeletal muscle radiation attenuation and basis of its biological variation. *Acta Physiol (Oxf)*. 2014;210(3):489-497. doi:10.1111/apha.12224
19. Endo K, Ichinose M, Kobayashi E, et al. Head and neck cancer and sarcopenia: an integrative clinical and functional review. *Cancers (Basel)*. 2024;16(20):3460. doi:10.3390/cancers16203460
20. Almada-Correia I, Neves PM, Mäkitie A, Ravasco P. Body composition evaluation in head and neck cancer patients: a review. *Front Oncol*. 2019;9:1112. doi:10.3389/fonc.2019.01112
21. Ye Z, Saraf A, Ravipati Y, et al. Development and validation of an automated image-based deep learning platform for sarcopenia assessment in head and neck cancer. *JAMA Netw Open*. 2023;6(8):e2328280. doi:10.1001/jamanetworkopen.2023.28280
22. Naser MA, Wahid KA, Grossberg AJ, et al. Deep learning auto-segmentation of cervical skeletal muscle for sarcopenia analysis in patients with head and neck cancer. *Front Oncol*. 2022;12:930432. doi:10.3389/fonc.2022.930432
23. Koitka S, Kroll L, Malamutmann E, Oezcelik A, Nensa F. Fully automated body composition analysis in routine CT imaging using 3D semantic segmentation convolutional neural networks. *Eur Radiol*. 2021;31(4):1795-1804. doi:10.1007/s00330-020-07147-3
24. Wasserthal J, Breit HC, Meyer MT, et al. TotalSegmentator: robust segmentation of 104 anatomic structures in CT images. *Radiol Artif Intell*. 2023;5(5):e230024. doi:10.1148/ryai.230024
25. Pölsterl S. scikit-survival: a library for time-to-event analysis built on top of scikit-learn. *J Mach Learn Res*. 2020;21(212):1-6. Accessed May 9, 2026. https://www.jmlr.org/papers/v21/20-729.html
26. Davidson-Pilon C. Lifelines: survival analysis in Python. *J Open Source Softw*. 2019;4(40):1317. doi:10.21105/joss.01317
27. Ellis LM, Bernstein DS, Voest EE, et al. American Society of Clinical Oncology perspective: raising the bar for clinical trials by defining clinically meaningful outcomes. *J Clin Oncol*. 2014;32(12):1277-1280. doi:10.1200/JCO.2013.53.8009
28. Azevedo MD, de Pinho NB, de Carvalho Padilha P, de Oliveira LC, Peres WAF. Clinical usefulness of the patient-generated subjective global assessment short form© for nutritional screening in patients with head and neck cancer: a multicentric study. *Ecancermedicalscience*. 2024;18:1662.
29. Dobs AS, Boccia RV, Croot CC, et al. Effects of enobosarm on muscle wasting and physical function in patients with cancer: a double-blind, randomised controlled phase 2 trial. *Lancet Oncol*. 2013;14(4):335-345. doi:10.1016/S1470-2045(13)70055-X
30. Zhang H, Garcia JM. Anamorelin hydrochloride for the treatment of cancer-anorexia-cachexia in NSCLC. *Expert Opin Pharmacother*. 2015;16(8):1245-1253. doi:10.1517/14656566.2015.1041500
31. Grimes DA, Schulz KF. Bias and causal associations in observational research. *Lancet*. 2002;359(9302):248-252. doi:10.1016/S0140-6736(02)07451-2
32. Culié D, Schiappa R, Pace-Loscos T, et al. Enteral nutrition during radiotherapy for oropharyngeal cancers: prevalence and prognostic factors based on HPV status (a GETTEC Study). *J Clin Med*. 2023;12(9):3169. doi:10.3390/jcm12093169
33. Locher JL, Bonner JA, Carroll WR, et al. Patterns of prophylactic gastrostomy tube placement in head and neck cancer patients: a consideration of the significance of social support and practice variation. *Laryngoscope*. 2013;123(8):1918-1925. doi:10.1002/lary.24022
34. Kamrath C, Blaurock M, Hoepfner N, et al. BOA-derived volumetric CT body composition provides prognostic information beyond BMI in surgically treated head and neck squamous cell carcinoma: a retrospective cohort study. *Cancers (Basel)*. 2026;18(15):2371. doi:10.3390/cancers18152371

© 2026 American Medical Association. All rights reserved, including those for text and data mining, AI training, and similar technologies.

Downloaded from jamanetwork.com by University of California - Los Angeles user on 10/08/2026

Supplemental Online Content

Jank E, Bang C, Raj, VB, et al. Body composition metrics and overall survival in head and neck cancer radiotherapy. *JAMA Otolaryngol Head Neck Surg*. Published online October 8, 2026. doi:10.1001/jamaoto.2026.2951

eMethods 1. EHR Data Collection

eMethods 2. Image Processing

eMethods 3. Cinematic Rendering

eMethods 4. Evaluation of Selection Bias and Sensitivity Analysis

eTable 1. Baseline demographics and clinical characteristics of patients treated with head and neck radiotherapy at our institution

eTable 2. Soft tissue volumes and normalized indices derived from CT simulation scans

eTable 3. Incremental prognostic performance of nested survival models for overall survival prediction

eTable 4. Baseline clinical and demographic characteristics of the imaging subcohort (n=659) and the excluded clinical cohort (n=528)

eTable 5. Multivariable Cox proportional hazards sensitivity analysis evaluating the impact of cohort inclusion status in the imaging subcohort on overall survival

eTable 6. Survival Follow-Up Statistics

eFigure 1. Fully automated pipeline for volumetric body composition phenotyping and prognostic modeling in head and neck cancer

eFigure 2. Representative tumor volume segmentations for quality assurance

eFigure 3. Representative skeletal muscle segmentations for quality assurance

eFigure 4. Representative subcutaneous adipose tissue segmentations for quality assurance

eFigure 5. Representative intermuscular adipose tissue segmentations for quality assurance

© 2026 American Medical Association. All rights reserved, including those for text and data mining, AI training, and similar technologies.

eFigure 6. Kaplan–Meier survival curve showing 5-year survival differences based on concurrent chemotherapy status

eFigure 7. Kaplan–Meier survival curve showing 5-year survival differences based on HPV/disease site

eFigure 8. Kaplan–Meier survival curve showing 5-year survival differences based on surgery status

eFigure 9. Kaplan–Meier survival curve showing 5-year survival differences based on age

eFigure 10. Kaplan–Meier survival curve showing 5-year survival differences based on ECOG performance status

eFigure 11. Kaplan–Meier survival curve showing 5-year survival differences based on disease stage

eFigure 12. Representative 3D cinematic rendering of automated volumetric body composition segmentation from pretreatment CT simulation imaging

eFigure 13. Relative volumetric tissue composition across baseline BMI categories within the imaging subcohort (n=659)

eFigure 14. Soft tissue ratios displayed by patient sorted from low to high BMI

eFigure 15. Distribution of soft tissue ratios sorted from low to high BMI for patients binned into 60 groups

eFigure 16. Covariate-adjusted survival curves illustrating survival trajectories associated with intermuscular adiposity index (IAI) and skeletal muscle index (SMI)

eFigure 17. Decision curve analysis evaluating the net clinical benefit of nested prognostic survival models across threshold probabilities for 5-year overall survival prediction

This supplemental material has been provided by the authors to give readers additional information about their work.

© 2026 American Medical Association. All rights reserved, including those for text and data mining, AI training, and similar technologies.

Online-Only Text

Supplemental Methods 1: EHR Data Collection

Electronic Health Record (EHR) data were extracted from the institutional clinical data warehouse. Demographic variables, including age, sex (assigned at birth), and survival outcomes, were retrieved from structured database tables. BMI was calculated using baseline height and weight measurements.

Age was modeled as a continuous variable using restricted cubic splices to handle non-linearity. Treatment year was zero-anchored and treated as a continuous variable. Smoking status was categorized using documented pack-year histories. Functional status was determined using Eastern Cooperative Oncology Group (ECOG) performance status or Karnofsky Performance Scale (KPS) scores extracted from clinical narratives using regular expression–based parsing logic. KPS values were converted to ECOG categories using standard clinical conversion methods, with manual chart review performed for ambiguous cases.

Surgical treatment was identified using relevant Current Procedural Terminology (CPT) codes within 10 weeks before CT simulation. Systemic therapy exposure was determined through identification of medications within the Antineoplastics drug class, with treatment timing categorized relative to CT simulation. Disease stage, primary tumor site, and human papillomavirus (HPV)/p16 status were confirmed through manual chart review. Tumor staging was retrospectively harmonized according to the American Joint Committee on Cancer (AJCC) 8th edition staging system.[25] Complete-case analysis was performed for multivariable modeling.

© 2026 American Medical Association. All rights reserved, including those for text and data mining, AI training, and similar technologies.

Supplemental Methods 2: Image Processing

TotalSegmentator was used to delineate total body volume, skeletal muscle, subcutaneous adipose tissue, and intermuscular adipose tissue on pretreatment CT imaging. Automated segmentation outputs underwent quality-control filtering based on anatomic plausibility and vertebral segmentation completeness. Scans with C2–C7 vertebral segmentation volumes below 100 mm^3 were excluded from the final imaging cohort for subsequent analysis due to failed or incomplete segmentations. To standardize anatomic coverage across heterogeneous simulation acquisitions, all scans were cropped at the inferior boundary of the T2 vertebral body contour.

Because the tumor burden may distort adjacent anatomy, we implemented a dosimetrically guided strategy for automated removal of the tumor volume. For treatment plans with a maximum prescription dose exceeding 67 Gy, identified from the RTPLAN data, the corresponding 95% isodose volume was delineated using the RTDOSE file. This high-dose volume was subtracted from soft tissue masks, effectively minimizing tumor contamination within the body composition measurements.

After processing, a random sample of scans underwent visual quality assurance review by a radiation oncologist to confirm the expected behavior of this pipeline. A subset of these CT images and soft tissue/tumor volume overlays are shown in **Supplemental Figures 2-5**. Raw tissue volumes and derived indices are summarized in **Supplemental Table 2**. To account for inter-patient variations in stature, tissue volumes (V) were normalized to patient height squared (h^2), yielding tissue indices expressed in cm^3/m^2:

$$Soft\ Tissue\ Index = \frac{V}{h^2}$$

Normalized indices were calculated for skeletal muscle, subcutaneous adipose tissue, and intermuscular adipose tissue, yielding the skeletal muscle index (SMI), subcutaneous adiposity index (SAI), and intermuscular adiposity index (IAI), respectively.

Continuous body composition variables were subsequently z-score standardized before multivariable modeling, enabling hazard ratios to represent the relative change in mortality risk associated with a 1-standard-deviation (SD) increase.

© 2026 American Medical Association. All rights reserved, including those for text and data mining, AI training, and similar technologies.

Supplemental Methods 3: Cinematic Rendering

Soft tissue compartments and the tumor volume were visualized through a 3D cinematic rendering generated using ParaView (version 6.1.0, Kitware Inc., Clifton Park, NY). Soft tissue volumes, including skeletal muscle, subcutaneous adipose tissue, and intermuscular adipose tissue, were autosegmented on the CT scan by TotalSegmentator. Volumes were cropped at the inferior boundary of the T2 vertebrae for each patient, standardizing the field-of-view across the cohort. Soft tissue contours for a sample patient were overlaid on the full CT scan for visualization. The planning tumor volume, approximated by the 95% isodose region, was also included in the rendering.

© 2026 American Medical Association. All rights reserved, including those for text and data mining, AI training, and similar technologies.

Supplemental Methods 4: Evaluation of Selection Bias and Sensitivity Analysis

To evaluate the potential for selection bias arising from missing or invalid CT Simulation imaging, a formal statistical comparison was conducted between the imaging subcohort (n=659) and excluded clinical patients (n=528). Continuous clinical variables were compared using the Mann-Whitney U test, and categorical variables were evaluated using Pearson's Chi-square test. Further, to confirm that missingness did not systematically bias survival estimates, a sensitivity analysis was performed on the entire cohort (n=1,187). A multivariable Cox proportional hazards regression model was constructed incorporating inclusion status in the imaging subcohort as an independent covariate. This allowed us to determine whether cohort exclusion independently impacted overall survival when controlling for baseline clinical variance.

© 2026 American Medical Association. All rights reserved, including those for text and data mining, AI training, and similar technologies.

Online-Only Tables

Supplemental Table 1. **Baseline demographics and clinical characteristics of patients treated with head and neck radiotherapy at our institution, where imaging was available (n=659).** Indentation signifies where categories were grouped for multivariable analysis.

Characteristic	Category (if applicable)	Overall (n = 659)
Age, years, median (range)		63.0 (5.0 - 100.0)
Sex, No. (%)	**Female**	167 (25.3)
	Male	492 (74.7)
BMI (kg/m²), median (range)		25.5 (12.9 - 47.8)
BMI Category, No. (%)	**Underweight (<18.5)**	18 (2.7)
	Healthy (18.5-24.9)	279 (42.3)
	Overweight (25-29.9)	231 (35.1)
	Obese (≥30)	131 (19.9)
Smoking Status, No. (%)	**Heavy (>=10 PY)**	93 (14.1)
	Moderate (<10 PY)	51 (7.7)
	Never Smoker	376 (57.1)
	Unknown	139 (21.2)
ECOG PS, No. (%)	**0 - Fully Active**	396 (60.1)
	1 - Restricted Activity	227 (34.4)
	2 + (2/3/4)	36 (5.5)
	2 - Ambulatory/Self-care	28 (4.2)
	3 - Limited Self-care	5 (0.8)
	4 - Completely Disabled	3 (0.5)
Primary Tumor Site, No. (%)	**Larynx/Hypopharynx**	78 (11.8)
	Nasopharynx/Sinus	44 (6.7)
	Oral Cavity	152 (23.1)
	Oropharynx	343 (52.0)
	Skin/Salivary/Thyroid	42 (6.4)
Disease Stage, No. (%)	**Stage 0/I**	147 (22.3)
	Stage 0	4 (0.6)
	Stage I	143 (21.7)
	Stage II	150 (22.8)
	Stage III	153 (23.2)
	Stage IV	209 (31.7)
HPV Status, No. (%)	**HPV+ OPC**	277 (42.0)
	HPV- OPC	51 (7.7)
	Non-OPC N/A	331 (50.2)

© 2026 American Medical Association. All rights reserved, including those for text and data mining, AI training, and similar technologies.

Characteristic	Category (if applicable)	Overall (n = 659)
Treatment Modality, No. (%)	**Definitive RT**	288 (43.7)
	Surgery + Adjuvant RT	371 (56.3)
Chemotherapy Regimen, No. (%)	**Concurrent**	311 (47.2)
	Concurrent + Adjuvant	4 (0.6)
	Concurrent Only	270 (41.0)
	Induction + Concurrent	37 (5.6)
	None/Induction/Salvage	348 (52.8)
	Induction Only	5 (0.8)
	No Systemic Therapy	249 (37.8)
	Salvage Chemo Only	94 (14.3)

***Abbreviations**: BMI, Body Mass Index; ECOG PS, Eastern Cooperative Oncology Group Performance Status; HPV, Human papillomavirus; OPC, Oropharyngeal cancer; RT, Radiation Therapy.*

© 2026 American Medical Association. All rights reserved, including those for text and data mining, AI training, and similar technologies.

Supplemental Table 2. Soft tissue volumes and normalized indices derived from CT simulation scans (n=659). Volumes extracted using 3D autosegmentation on T2-cropped CT scans, with tumor volume excluded. Volume indices were calculated by normalizing absolute volumes to patient height squared.

Tissue Volumes and Derived Metrics, median (range)	
Total Body Volume (cm^3)	8416.0 (3206.4 - 16702.4)
Skeletal Muscle Volume (cm^3)	2456.3 (491.7 - 5589.3)
Subcutaneous Adipose Tissue Volume (cm^3)	1454.4 (185.5 - 6805.1)
Intermuscular Adipose Tissue Volume (cm^3)	388.9 (37.1 - 1289.5)
Tumor Volume (cm^3)	158.3 (15.1 - 951.4)
Skeletal Muscle Index (cm^3/m^2)	804.5 (379.2 - 1740.6)
Subcutaneous Adiposity Index (cm^3/m^2)	478.5 (57.8 - 2349.7)
Intermuscular Adiposity Index (cm^3/m^2)	127.9 (21.7 - 419.8)

© 2026 American Medical Association. All rights reserved, including those for text and data mining, AI training, and similar technologies.

Supplemental Table 3: Incremental prognostic performance of nested survival models for overall survival prediction.

Model	Included Variables	C-index (95% CI)	ΔC-index vs CBM
Clinical Baseline Model (CBM)	Age, sex, smoking, ECOG PS, stage, HPV/site, surgery, chemotherapy	0.714 (0.679–0.750)	0
CBM + BMI	CBM + BMI	0.716 (0.679–0.755)	+0.002
CBM + Tissue Indices	CBM + SMI + IAI	0.725 (0.689–0.759)	+0.011
Combined Model	CBM + BMI + SMI + IAI	0.733 (0.697–0.768)	+0.019

Abbreviations: *BMI, body mass index; CBM, clinical baseline model; ECOG PS, Eastern Cooperative Oncology Group Performance Status; HPV, human papillomavirus; IAI, intermuscular adiposity index; SMI, skeletal muscle index; C-index, concordance index; CI, confidence interval.*

© 2026 American Medical Association. All rights reserved, including those for text and data mining, AI training, and similar technologies.

Supplemental Table 4: Baseline clinical and demographic characteristics of the imaging subcohort (n=659) and the excluded clinical cohort (n=528). Continuous variables compared using the Mann-Whitney U test. Categorical variables compared using Pearson's Chi-square test. This comparison between cohorts was conducted to investigate unmeasured selection bias in this study.

Characteristic	Category	Included Cohort (n=659)	Excluded Cohort (n=528)	P-Value
Age, years	**Median [IQR]**	63.0 [54.0 - 71.0]	64.0 [55.0 - 74.0]	0.0049
BMI (kg/m²)	**Median [IQR]**	25.5 [22.9 - 28.7]	25.5 [22.9 - 28.9]	0.9195
Sex				0.1207
	Female	167 (25.3%)	156 (29.5%)	
	Male	492 (74.7%)	372 (70.5%)	
Smoking Status				0. 6954
	Heavy (>=10 PY)	93 (14.1%)	83 (15.7%)	
	Moderate (<10 PY)	51 (7.7%)	44 (8.3%)	
	Never Smoker	376 (57.1%)	302 (57.2%)	
	Unknown	136 (21.1%)	99 (18/8%)	
HPV Status				<0.001
	HPV+ OPC	276 (41.9%)	90 (17.0%)	
	HPV- OPC	51 (7.7%)	20 (3.8%)	
	Non-OPC	332 (50.4%)	418 (79.2%)	
Disease Stage				0.0047
	Stage 0-I	147 (22.3%)	89 (16.9%)	
	Stage II	150 (22.8%)	109 (20.6%)	
	Stage III	153 (23.2%)	112 (21.2%)	
	Stage IV	209 (31.7%)	218 (41.3%)	
Chemotherapy Regimen				<0.001
	Concurrent	311 (47.2%)	150 (28.4%)	
	No Systemic + Induction + Salvage	348 (52.8%)	378 (71.6%)	
ECOG PS				<0.001
	0 - Fully Active	396 (60.1%)	235 (44.5%)	
	1 - Restricted Activity	227 (34.4%)	240 (45.5%)	
	2-4 - Limited/Restricted Self-care	36 (5.5%)	53 (10.0%)	
Treatment Modality				<0.001
	Definitive RT	288 (43.7%)	286 (54.2%)	
	Surgery + Adjuvant RT	371 (56.3%)	242 (45.8%)	

***Abbreviations**: IQR, Interquartile Range; PY, pack-year; BMI, Body Mass Index; ECOG PS, Eastern Cooperative Oncology Group Performance Status; HPV, Human papillomavirus; OPC, Oropharyngeal cancer; RT, Radiation Therapy.*

© 2026 American Medical Association. All rights reserved, including those for text and data mining, AI training, and similar technologies.

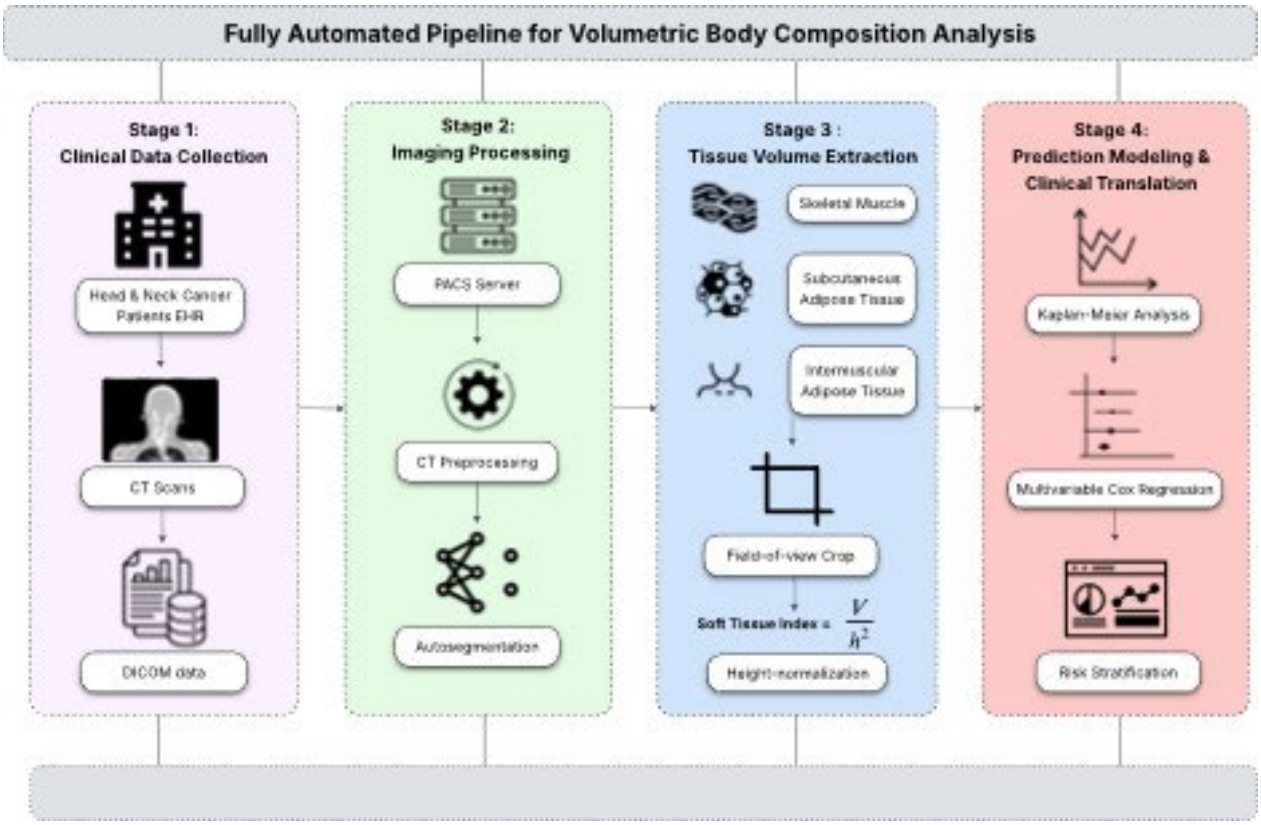
Supplemental Table 5: Multivariable Cox proportional hazards sensitivity analysis evaluating the impact of cohort inclusion status in the imaging subcohort on overall survival. The entire clinical cohort (n=1,187) is investigated to formally evaluate the risk of selection bias due to cohort differences between the larger clinical cohort and imaging subcohort.

Clinical Variable	Adjusted HR	95% CI	P-value
Cohort Inclusion Status (Included vs. Excluded)	0.84	0.67 - 1.04	0.108
Age (Continuous)	1.02	1.02 - 1.03	<0.001
Baseline BMI (Continuous)	0.96	0.93 - 0.98	<0.001
Sex, Male	1.20	0.94 - 1.52	0.137
Smoking Status, Unknown	1.09	0.83-1.43	0.530
Smoking Status, Moderate	1.06	0.74-1.53	0.742
Smoking Status, Heavy	1.23	0.94-1.62	0.126
HPV Status, HPV- OPC	2.13	1.51 - 2.99	<0.001
HPV Status, HPV+ OPC	0.58	0.44 - 0.76	<0.001
Disease Stage, Stage II	1.00	0.70 - 1.44	0.997
Disease Stage, Stage III	1.42	1.02 – 1.99	0.039
Disease Stage, Stage IV	1.59	1.16 - 2.18	0.004
Chemotherapy Regimen, Concurrent	0.79	0.63 - 0.99	0.041
ECOG PS, 1 - Restricted Activity	1.46	1.17 - 1.81	<0.001
ECOG PS, 2-4 - Limited/Restricted Self-care	2.07	1.47 - 2.93	<0.001
Treatment Modality, Surgery + Adjuvant RT	0.86	0.70 - 1.07	0.171

***Abbreviations**: HR, Hazard Ratio; CI, Confidence Interval; BMI, Body Mass Index; PY, pack-year; HPV, Human papillomavirus; OPC, Oropharyngeal cancer; ECOG PS, Eastern Cooperative Oncology Group Performance Status; RT, Radiation Therapy.*

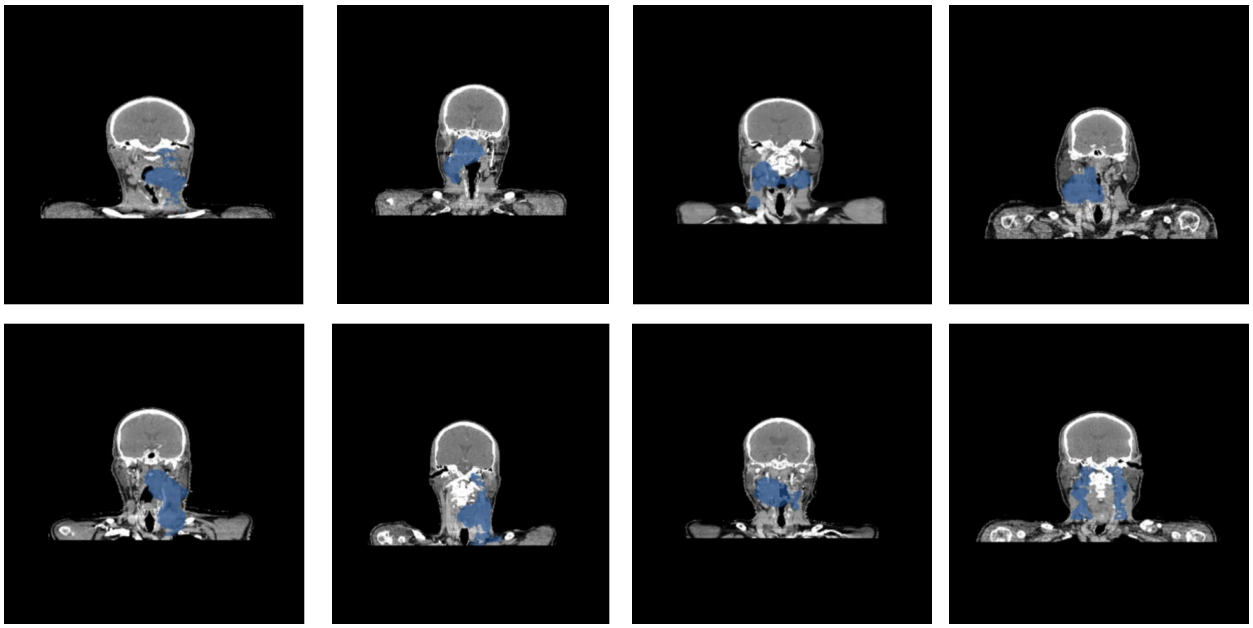
***Reference groups:** Excluded cohort, Female, Never Smoker, Non-OPC, Stage 0-1, No Systemic Therapy, ECOG 0, Definitive RT.*

© 2026 American Medical Association. All rights reserved, including those for text and data mining, AI training, and similar technologies.



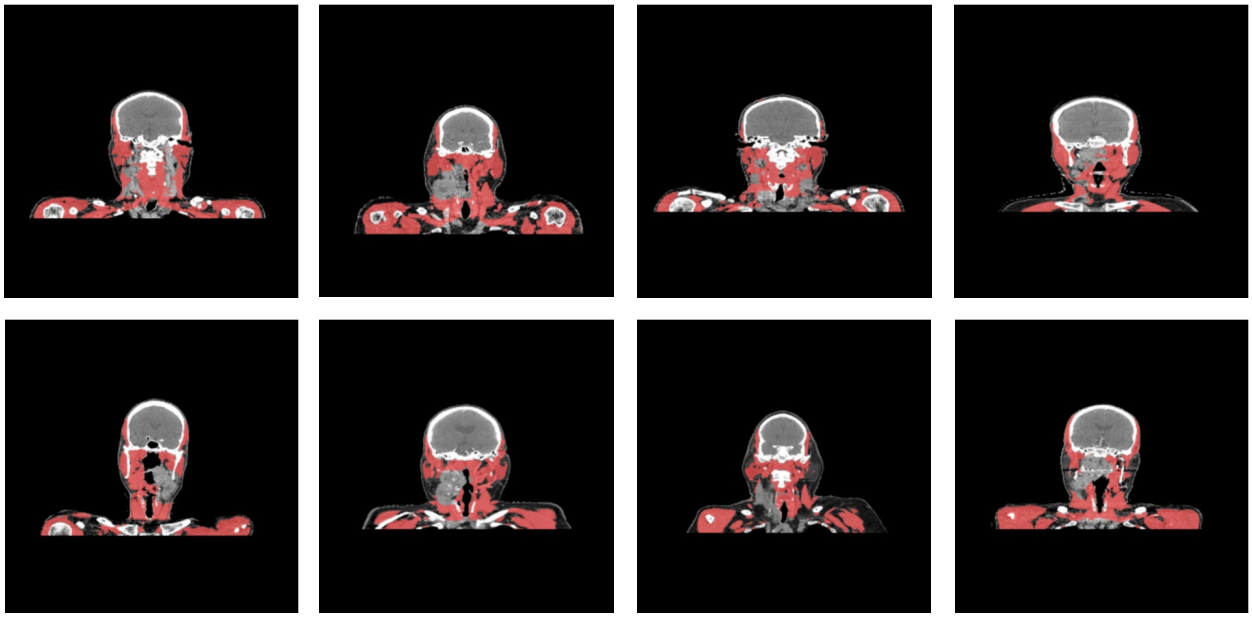
Supplemental Figure 1. Fully automated pipeline for volumetric body composition phenotyping and prognostic modeling in head and neck cancer. Overview of the computational workflow integrating electronic health record (EHR) data, radiotherapy planning data, and pretreatment CT simulation imaging for automated volumetric body composition analysis. CT simulation scans underwent preprocessing and deep learning-based autosegmentation using TotalSegmentator, followed by extraction and normalization of skeletal muscle, subcutaneous adipose tissue, and intermuscular adipose tissue volumes. Imaging-derived biomarkers were subsequently incorporated into survival modeling and risk stratification analyses.

© 2026 American Medical Association. All rights reserved, including those for text and data mining, AI training, and similar technologies.



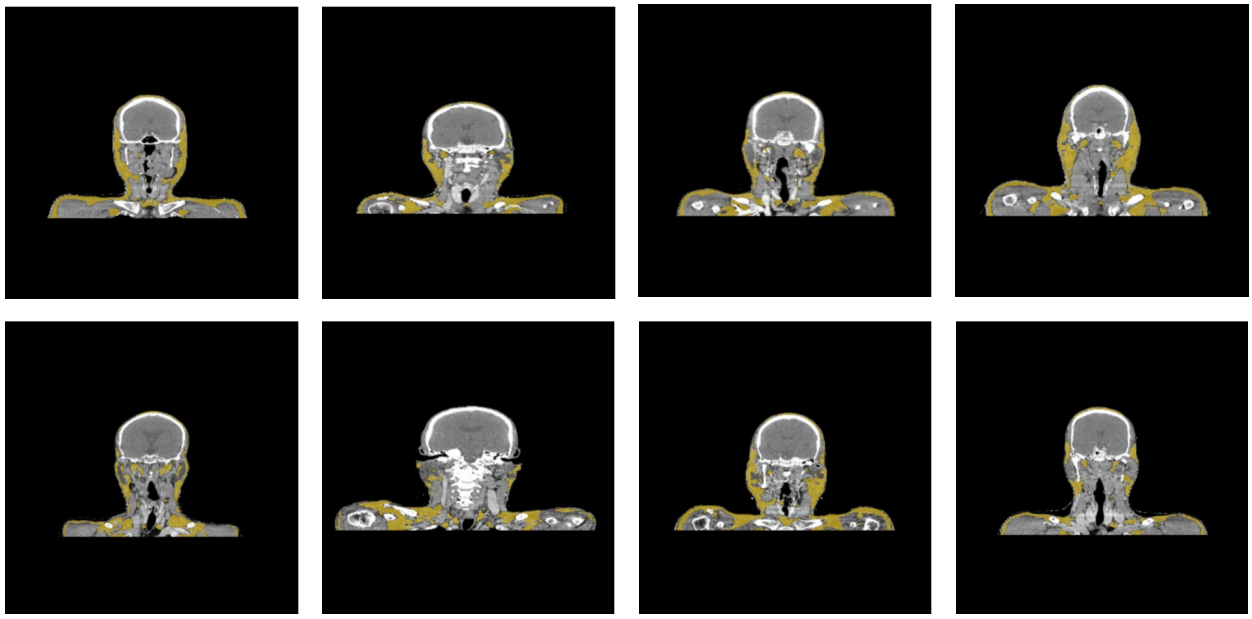
Supplemental Figure 2. Representative tumor volume segmentations for quality assurance. CT Simulation scans from eight unique patients demonstrating the tumor volume (blue overlay). Visual validation was performed to qualitatively assess the validity of these volumes prior to subtraction from the surrounding soft-tissue compartments.

© 2026 American Medical Association. All rights reserved, including those for text and data mining, AI training, and similar technologies.



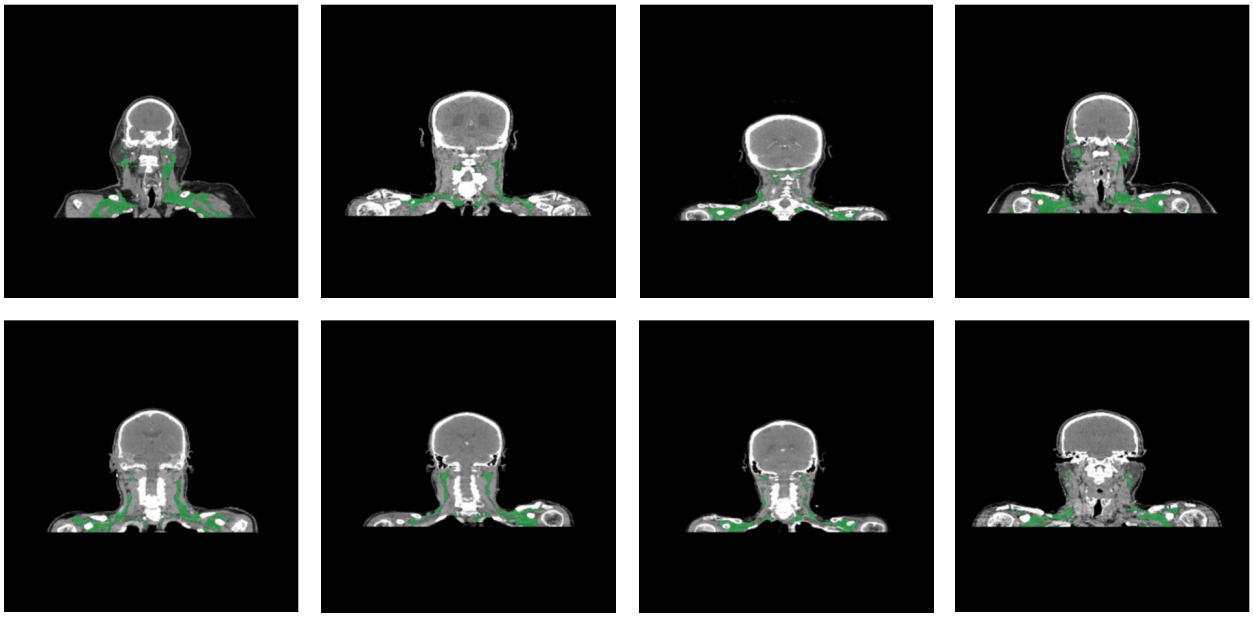
Supplemental Figure 3. Representative skeletal muscle segmentations for quality assurance. CT Simulation scans from eight unique patients demonstrating the skeletal muscle area (red overlay). Visual validation was performed to confirm the accurate delineation of muscle boundaries required for subsequent analysis.

© 2026 American Medical Association. All rights reserved, including those for text and data mining, AI training, and similar technologies.



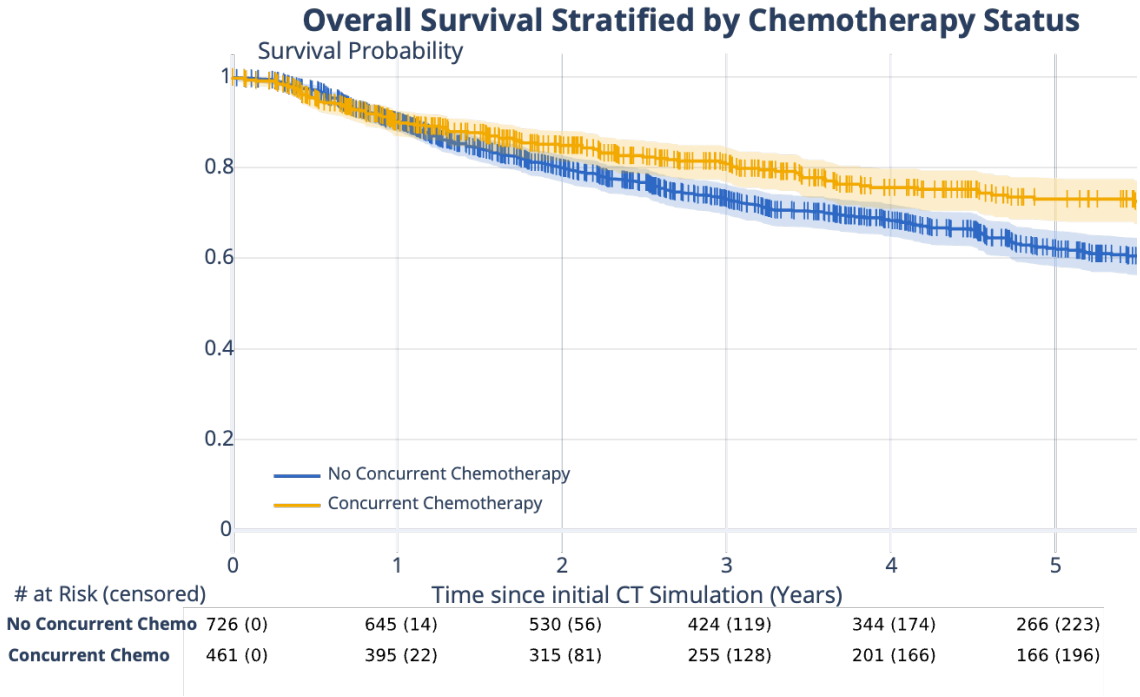
Supplemental Figure 4. Representative subcutaneous adipose tissue segmentations for quality assurance. CT Simulation scans from eight unique patients demonstrating the subcutaneous adipose tissue area (yellow overlay). Visual validation was performed to confirm the accurate delineation of soft tissue boundaries required for subsequent analysis.

© 2026 American Medical Association. All rights reserved, including those for text and data mining, AI training, and similar technologies.



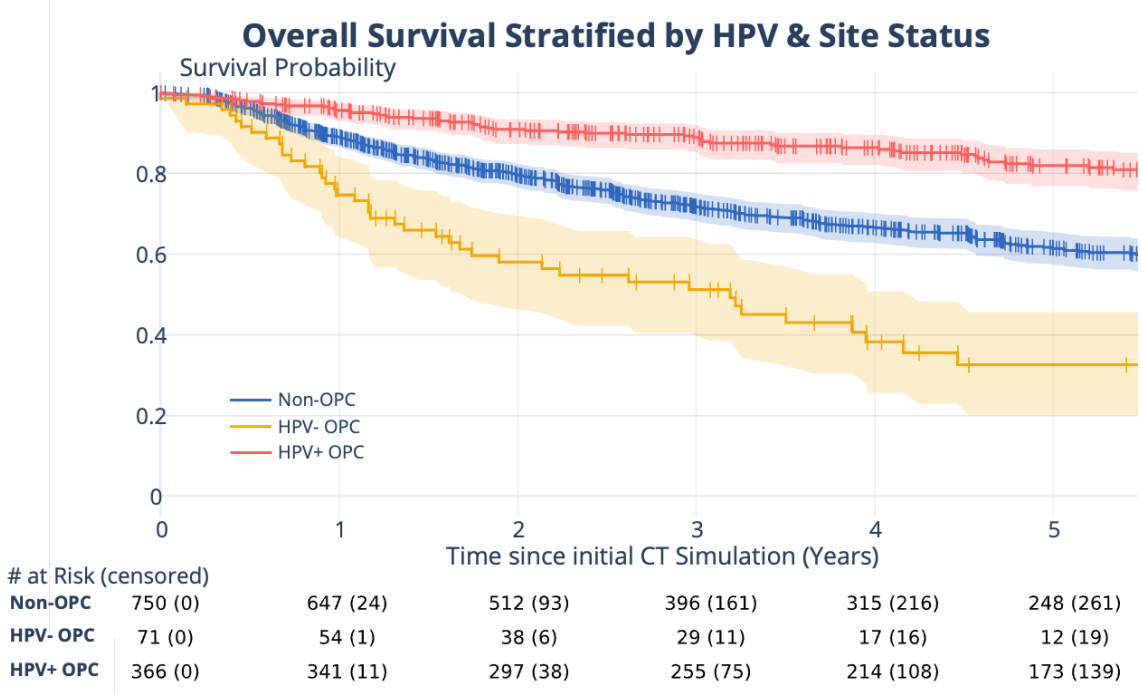
Supplemental Figure 5. Representative intermuscular adipose tissue segmentations for quality assurance. CT Simulation scans from eight unique patients demonstrating the intermuscular adipose tissue area (green overlay). Visual validation was performed to confirm the accurate delineation of soft tissue boundaries required for subsequent analysis.

© 2026 American Medical Association. All rights reserved, including those for text and data mining, AI training, and similar technologies.



Supplemental Figure 6. Kaplan–Meier survival curve showing 5-year survival differences based on concurrent chemotherapy status for n=1,187. Time zero represents the date of CT Simulation. The number of patients at risk at each yearly interval is provided in the table below the plot. Shaded regions represent 95% confidence intervals.

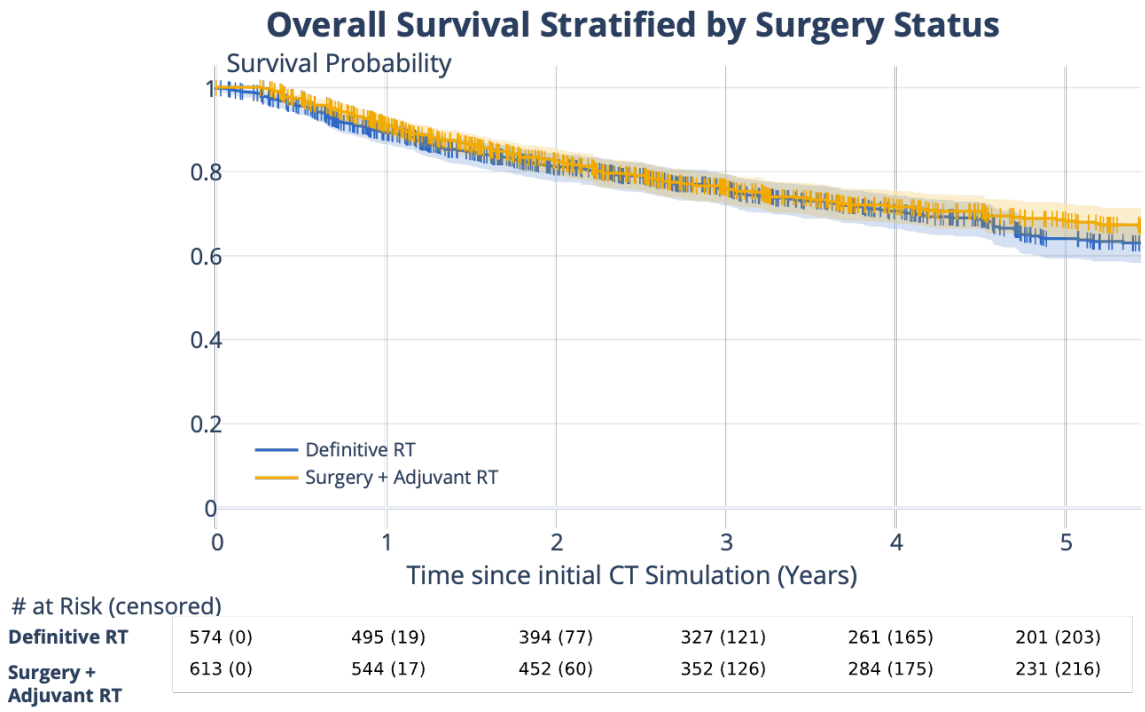
© 2026 American Medical Association. All rights reserved, including those for text and data mining, AI training, and similar technologies.



# at Risk (censored)						
Non-OPC	750 (0)	647 (24)	512 (93)	396 (161)	315 (216)	248 (261)
HPV- OPC	71 (0)	54 (1)	38 (6)	29 (11)	17 (16)	12 (19)
HPV+ OPC	366 (0)	341 (11)	297 (38)	255 (75)	214 (108)	173 (139)

Supplemental Figure 7. Kaplan–Meier survival curve showing 5-year survival differences based on HPV/disease site for n=1,187. Time zero represents the date of CT Simulation. The number of patients at risk at each yearly interval is provided in the table below the plot. Shaded regions represent 95% confidence intervals.

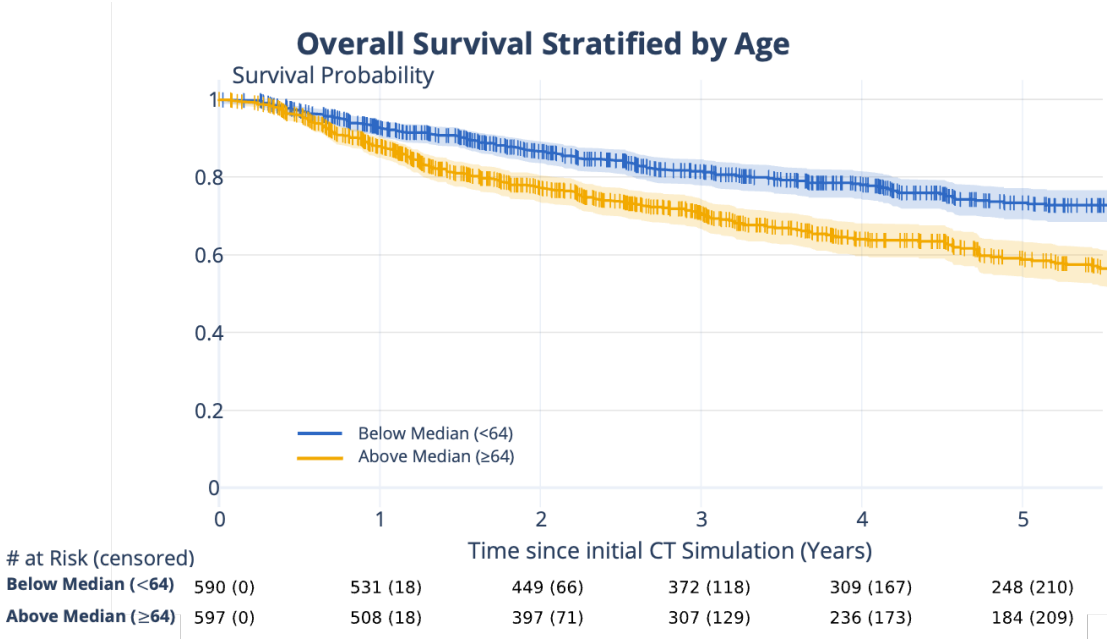
© 2026 American Medical Association. All rights reserved, including those for text and data mining, AI training, and similar technologies.



# at Risk (censored)						
Definitive RT	574 (0)	495 (19)	394 (77)	327 (121)	261 (165)	201 (203)
Surgery + Adjuvant RT	613 (0)	544 (17)	452 (60)	352 (126)	284 (175)	231 (216)

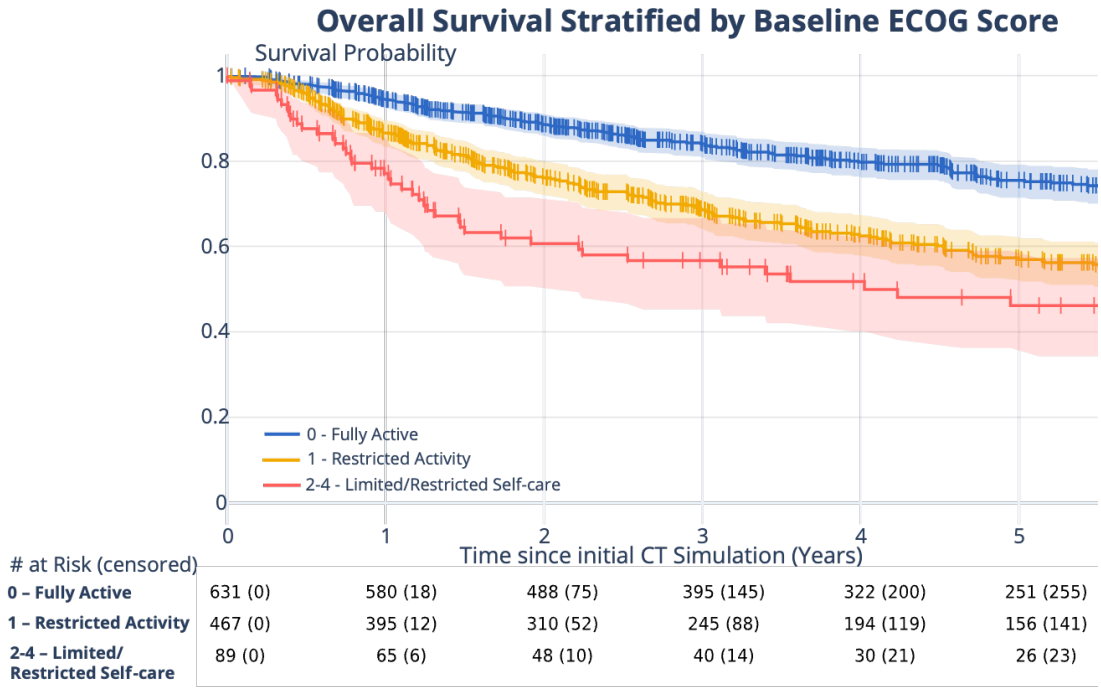
Supplemental Figure 8. Kaplan–Meier survival curve showing 5-year survival differences based on surgery status for n=1,187. Time zero represents the date of CT Simulation. The number of patients at risk at each yearly interval is provided in the table below the plot. Shaded regions represent 95% confidence intervals.

© 2026 American Medical Association. All rights reserved, including those for text and data mining, AI training, and similar technologies.



Supplemental Figure 9. Kaplan–Meier survival curve showing 5-year survival differences based on age for n=1,187. Time zero represents the date of CT Simulation. The number of patients at risk at each yearly interval is provided in the table below the plot. Shaded regions represent 95% confidence intervals.

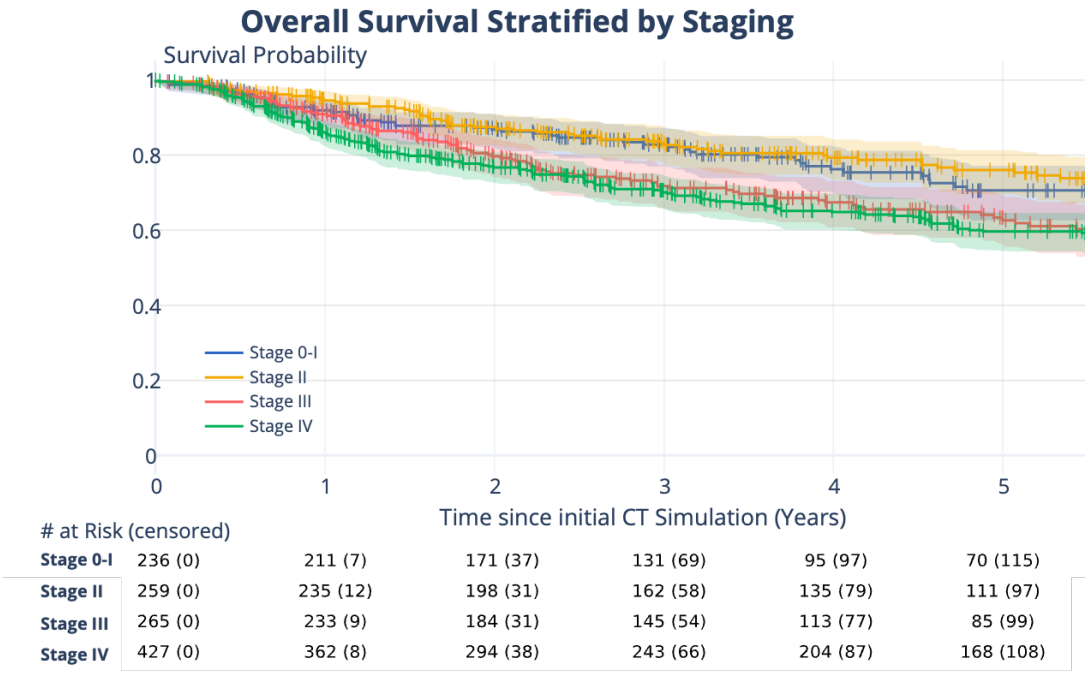
© 2026 American Medical Association. All rights reserved, including those for text and data mining, AI training, and similar technologies.



# at Risk (censored)						
0 – Fully Active	631 (0)	580 (18)	488 (75)	395 (145)	322 (200)	251 (255)
1 – Restricted Activity	467 (0)	395 (12)	310 (52)	245 (88)	194 (119)	156 (141)
2-4 – Limited/ Restricted Self-care	89 (0)	65 (6)	48 (10)	40 (14)	30 (21)	26 (23)

Supplemental Figure 10. Kaplan–Meier survival curve showing 5-year survival differences based on ECOG performance status for n=1,187. Time zero represents the date of CT Simulation. The number of patients at risk at each yearly interval is provided in the table below the plot. Shaded regions represent 95% confidence intervals.

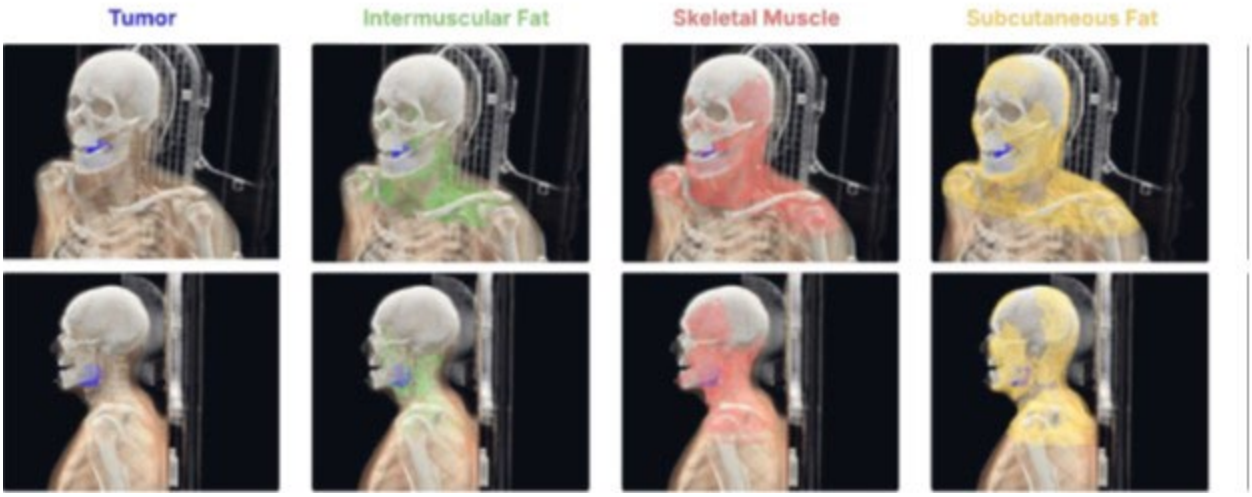
© 2026 American Medical Association. All rights reserved, including those for text and data mining, AI training, and similar technologies.



# at Risk (censored)						
Stage 0-I	236 (0)	211 (7)	171 (37)	131 (69)	95 (97)	70 (115)
Stage II	259 (0)	235 (12)	198 (31)	162 (58)	135 (79)	111 (97)
Stage III	265 (0)	233 (9)	184 (31)	145 (54)	113 (77)	85 (99)
Stage IV	427 (0)	362 (8)	294 (38)	243 (66)	204 (87)	168 (108)

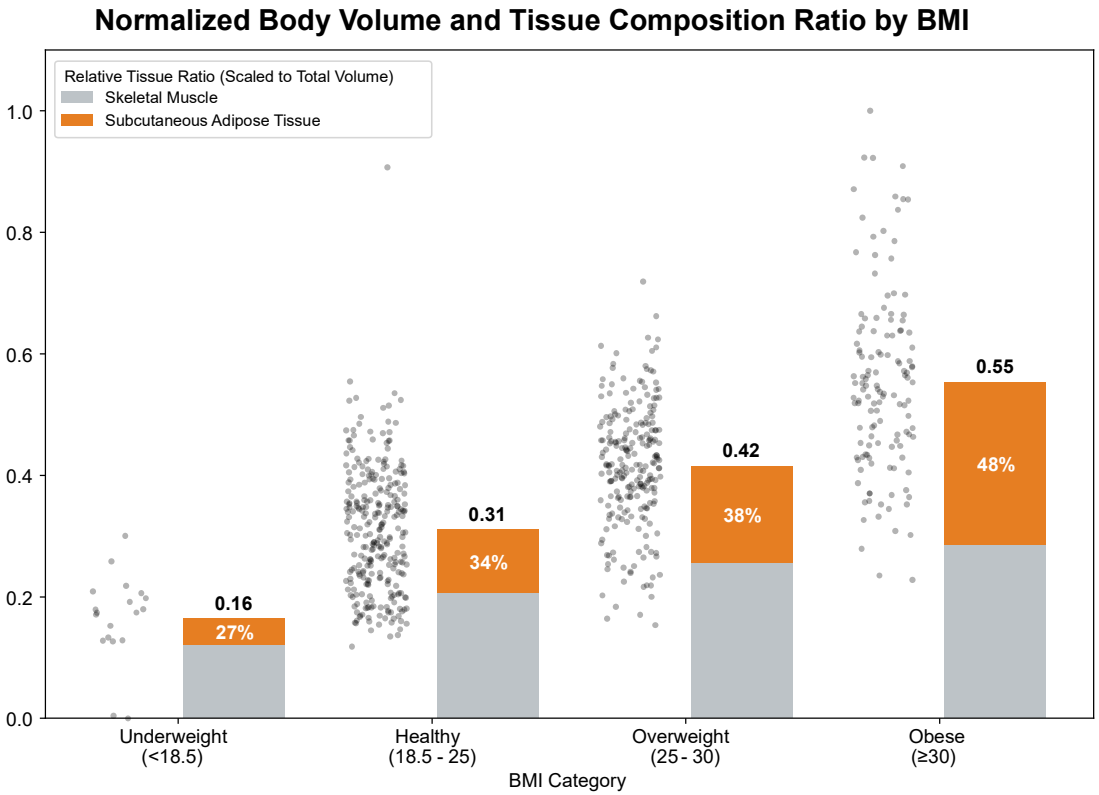
Supplemental Figure 11. Kaplan–Meier survival curve showing 5-year survival differences based on disease stage for n=1,187. Time zero represents the date of CT Simulation. The number of patients at risk at each yearly interval is provided in the table below the plot. Shaded regions represent 95% confidence intervals.

© 2026 American Medical Association. All rights reserved, including those for text and data mining, AI training, and similar technologies.



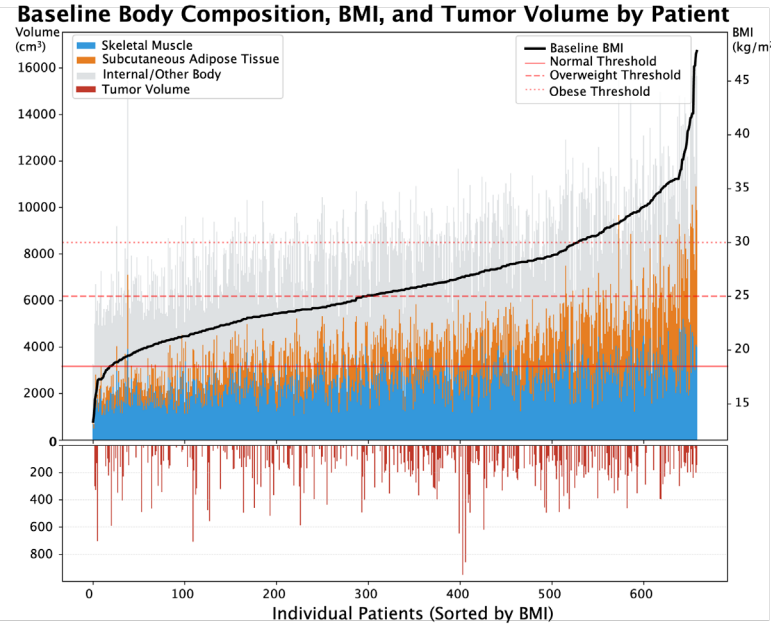
Supplemental Figure 12. Representative 3D cinematic rendering of automated volumetric body composition segmentation from pretreatment CT simulation imaging. Tumor volume was approximated from the 95% isodose region derived from the RTDOSE file. Soft tissue compartments, including intermuscular adipose tissue (fat), skeletal muscle, and subcutaneous adipose tissue (fat) were automatically segmented using TotalSegmentator following T2-level cropping standardization.

© 2026 American Medical Association. All rights reserved, including those for text and data mining, AI training, and similar technologies.



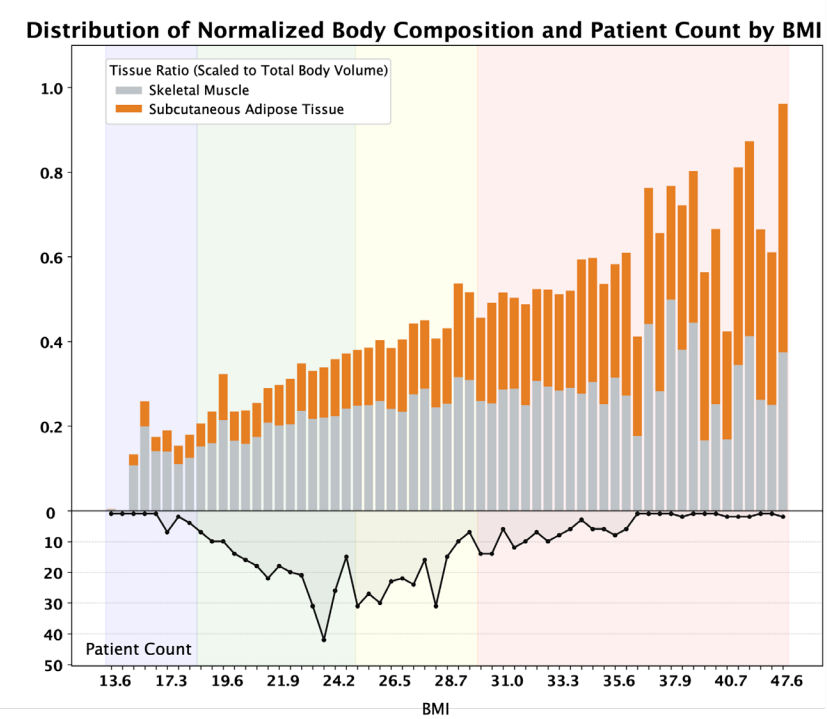
Supplemental Figure 13. Relative volumetric tissue composition across baseline BMI categories within the imaging subcohort (n=659). Bars represent normalized total body volume partitioned into skeletal muscle and subcutaneous adipose tissue components. White labels indicate the relative proportion of adipose tissue within each BMI category, while black labels indicate the mean normalized total tissue volume. Individual gray dots represent patient-level normalized total body volumes.

© 2026 American Medical Association. All rights reserved, including those for text and data mining, AI training, and similar technologies.



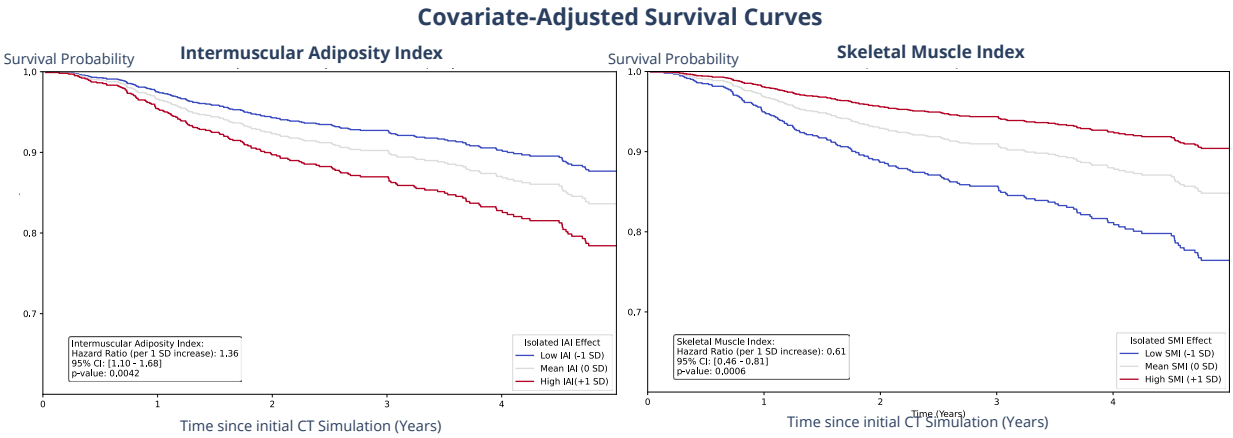
Supplemental Figure 14. Soft tissue ratios displayed by patient sorted from low to high BMI. The inverted plot displays planning tumor volume extracted for each patient. Different colors denote different tissue compartments, as indicated by the legend in the top left. BMI category thresholds are shown by horizontal red lines, as indicated by the legend in the top right.

© 2026 American Medical Association. All rights reserved, including those for text and data mining, AI training, and similar technologies.



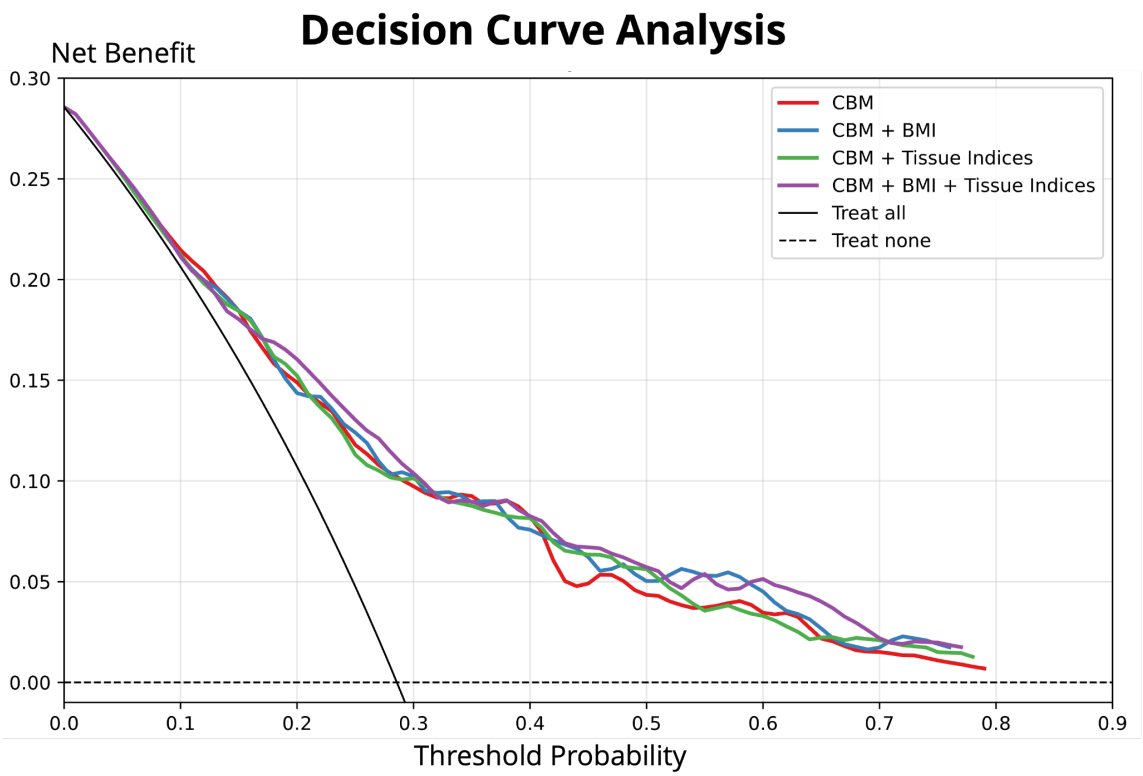
Supplemental Figure 15. Distribution of soft tissue ratios sorted from low to high BMI for patients binned into 60 groups. Soft tissue compartments are indicated by the legend in the top left. The inverted plot shows the true patient count represented for each bin. BMI categories are colored, with purple indicating Underweight, green as Healthy, yellow as Overweight, and red as Obese.

© 2026 American Medical Association. All rights reserved, including those for text and data mining, AI training, and similar technologies.



Supplemental Figure 16. Covariate-adjusted survival curves illustrating survival trajectories associated with intermuscular adiposity index (IAI) and skeletal muscle index (SMI). Predicted survival probabilities were estimated from multivariable Cox regression models for hypothetical patient profiles representing low (-1 SD), mean (0 SD), and high (+1 SD) tissue index distributions while holding all remaining covariates at baseline.

© 2026 American Medical Association. All rights reserved, including those for text and data mining, AI training, and similar technologies.



Supplemental Figure 17. Decision curve analysis evaluating the net clinical benefit of nested prognostic survival models across threshold probabilities for 5-year overall survival prediction. Models incorporating imaging-derived tissue biomarkers demonstrated greater net clinical benefit across clinically relevant threshold probabilities compared with the clinical baseline model (CBM).

© 2026 American Medical Association. All rights reserved, including those for text and data mining, AI training, and similar technologies.

Data Sharing Statement

Jank. Body Composition Metrics and Overall Survival in Head and Neck Cancer Radiotherapy. *JAMA Otolaryngol Head Neck Surg*. Published October 08, 2026. doi:10.1001/jamaoto.2026.2951

Data
Data available: No

Additional Information
Explanation for why data not available: Data and statistical code supporting the findings of this study are available from the corresponding author upon reasonable academic request. The autosegmentation tool utilized in this pipeline is an open-source framework, detailed in the Methods section. Data may be made available by contacting the author.